Downloaded from orbit.dtu.dk on: Dec 17, 2017

Technical University of Denmark

New data on eudialyte decomposition minerals from kakortokites and associated pegmatites of the Ilimaussaq complex, South Greenland

Karup-Møller, Sven; Rose-Hansen, John

Published in:
Geological Society of Denmark. Bulletin

Publication date:
2013

Document Version
Publisher's PDF, also known as Version of record

Link back to DTU Orbit

Citation (APA):
Karup-Møller, S., & Rose-Hansen, J. (2013). New data on eudialyte decomposition minerals from kakortokites and associated pegmatites of the Ilimaussaq complex, South Greenland. Geological Society of Denmark. Bulletin, 61, 47-70.

DTU Library
Technical Information Center of Denmark

General rights
Copyright and moral rights for the publications made accessible in the public portal are retained by the authors and/or other copyright owners and it is a condition of accessing publications that users recognise and abide by the legal requirements associated with these rights.

- Users may download and print one copy of any publication from the public portal for the purpose of private study or research.
- You may not further distribute the material or use it for any profit-making activity or commercial gain
- You may freely distribute the URL identifying the publication in the public portal

If you believe that this document breaches copyright please contact us providing details, and we will remove access to the work immediately and investigate your claim.

New data on eudialyte decomposition minerals from kakortokites and associated pegmatites of the Ilímaussaq complex, South Greenland*

SVEN KARUP-MØLLER & JOHN ROSE-HANSEN

Karup-Møller, S. & Rose-Hansen, J. 2013. New data on eudialyte decomposition minerals from kakortokites and associated pegmatites of the Ilímaussaq complex, South Greenland. ©2013 by Bulletin of the Geological Society of Denmark, Vol. 61, pp. 47–70. ISSN 2245-7070. (www.2dgf.dk/publikationer/bulletin).

A suite of samples with eudialyte and eudialyte decomposition minerals from the kakortokite and associated pegmatites of the Ilímaussaq complex in South Greenland has been investigated by electron microprobe analysis. Extensive decomposition of eudialyte has resulted in the formation of catapleiite as host for a number of rare and hitherto unknown REE minerals besides known minerals such as monazite and kainosite. Mineral A1 is present in very small amounts in nearly all eudialyte decomposition aggregates and comprises two varieties: Ca-rich A1 with composition $HCa_3REE_6(SiO_4)_6(F\square)$ and presumed apatite structure, and Ca-poor A1 with composition $(Fe,Mn,Ca)_{1.5}REE_6Si_6FO_{22}$ and unknown structure. Mineral A2 with composition $(Ca,Fe)_{1.2}REE_4Si_6O_{19-y}(OH)_{2y} \cdot nH_2O$ is indistinguishable from A1 in EMP-backscattered light and has only been found at a limited number of localities. Mineral A2 also occurs as a primary mineral at one locality. Additional rare and new REE-minerals are mineral A3 with composition $Na_{0.2}Ca_{0.6}Fe_{0.2}Mn_{0.5}Al_{0.5}REE_{2.8}Si_6F_{0.5}O)_{18-y}(OH)_{2y} \cdot nH_2O$; mineral Uk2 with composition $REE_{2.00}F_{1.50}O_{2.25-y}(OH)_{2y} \cdot nH_2O$; mineral Uk3 with composition $CaREE_4O_{7-y}OH)_{2y} \cdot nH_2O$; and mineral Y1 with composition $Na_2Ca_4Y_{2.7}REE_{1.3}F_{18}(OH)_4$. The Ce:(Y+La+Pr+Nd+Sm+Gd) molar ratio for A1, A2, A3, Uk2, Uk3 and monazite is close to 1:1. Characteristic for A1, A2 and monazite are substantial solid solutions between La and (Pr+Nd+Sm+Gd) with slowly increasing content of Ce as the content of La increases. A similar pattern does not exist for the REE in fresh eudialyte. Kainosite, identified in one decomposition aggregate, has not previously been found in the Ilímaussaq complex.

Keywords: Greenland, Ilímaussaq, kakortokite, pegmatite, eudialyte decomposition, unknown REE-mineral, monazite, kainosite, apatite group.

S.Karup-Møller [svka@byg.dtu.dk], Department of Civil Engineering, Technical University of Denmark, Brovej, Bygning 118, DK-2800 Lyngby, Denmark. J. Rose-Hansen [rose-hansen@dadlnet.dk], Department of Geoscience and Natural Resource Management, University of Copenhagen, Øster Voldgade 10, DK-1350 Copenhagen K, Denmark.

Received 13 February 2013
Accepted in revised form
22 November 2013
Published online
20 December 2013

*Contribution to the mineralogy of Ilímaussaq no. 143

Increasing demand for rare elements such as Zr, Nb, Ta and the rare earth elements (REE) for the manufacturing of a wide range of advanced materials has emphasized the need for new ore deposits with these elements. Until now these elements were mainly produced from carbonatitic rocks and as by-products from zircon and monazite in beach sands. One of the World's largest deposits of these elements is found in the peralkaline rocks of the Ilímaussaq complex in South Greenland. Estimated resources of some elements in Ilímaussaq are listed in Sørensen (1992).

Peralkaline nepheline syenites, termed "agpaitic" by Ussing (1912), were first described from the Ilímaussaq alkaline complex in South Greenland. Sørensen (1960) redefined agpaitic rocks as peralkaline rocks with chemically complex Zr-Ti silicate minerals such as eudialyte and rinkite instead of the chemically simpler zircon, titanite and ilmenite. Agpaitic rocks have high contents of Na-bearing minerals such as nepheline, arfvedsonite, aegirine, sodalite, eudialyte, steenstrupine and villiaumite (see Table 1 in Sørensen 1992). The most highly developed agpaitic rocks crystallized at very low temperatures. Eudialyte may be termed the type mineral of these rocks (Sørensen 1992).

Eudialyte is the main REE-bearing mineral in the

Ilímaussaq complex. Here the mineral contains 11–14 wt% ZrO_2, 1.7–8.7 wt% REE_2O_3 (Gerasimovsky 1969) and ~1 wt% Nb_2O_5. Eudialyte is a major mineral in the roof zone rocks where it occurs as an interstitial mineral (Bohse *et al*. 1974), and also in the lowest exposed zone of the complex, the kakortokites, where it is a liquidus cumulative mineral.

Extensive decomposition of eudialyte throughout the Ilímaussaq complex has taken place. The two major eudialyte alteration minerals are catapleiite and zircon, as originally described by Ussing (1898) and later summarized and confirmed by Sørensen (1962) and Karup-Møller *et al*. (2010). It is assumed that the formation of catapleiite was caused by residual interstitial liquids at a late magmatic stage whereas the formation of zircon was caused by liquids of external origin (Ussing 1898; Karup-Møller *et al*. 2010). The major eudialyte alteration mineral from the kakortokite area is catapleiite. Alteration of eudialyte in the marginal pegmatite of Ilímaussaq has, in addition to catapleiite and zircon, led to the formation of a number of rare, known and hitherto unknown, minerals present in very small amounts and with grain sizes generally less than 10 μm. These include fergusonite-(Ce), fergusonite-(Y), allanite, monazite, apatite, fersmite, nacareniobsite-(Ce), minerals A1, A2, Nb1, Nb2, Uk1 and Uk2 (Karup-Møller *et al*. 2010). Graser & Markl (2008) have in veins east of the Ilímaussaq complex found allanite as an alteration product after eudialyte.

This paper presents a study of altered eudialyte from eudialyte-rich layers in the kakortokite series and from hydrothermal mineral veins and pegmatites associated with the kakortokites. The study has yielded additional information on the alteration minerals A1, A2, Uk2, monazite, fergusonite-(Ce), fergusonite-(Y) and kainosite-(Y). Two new REE-minerals, A3

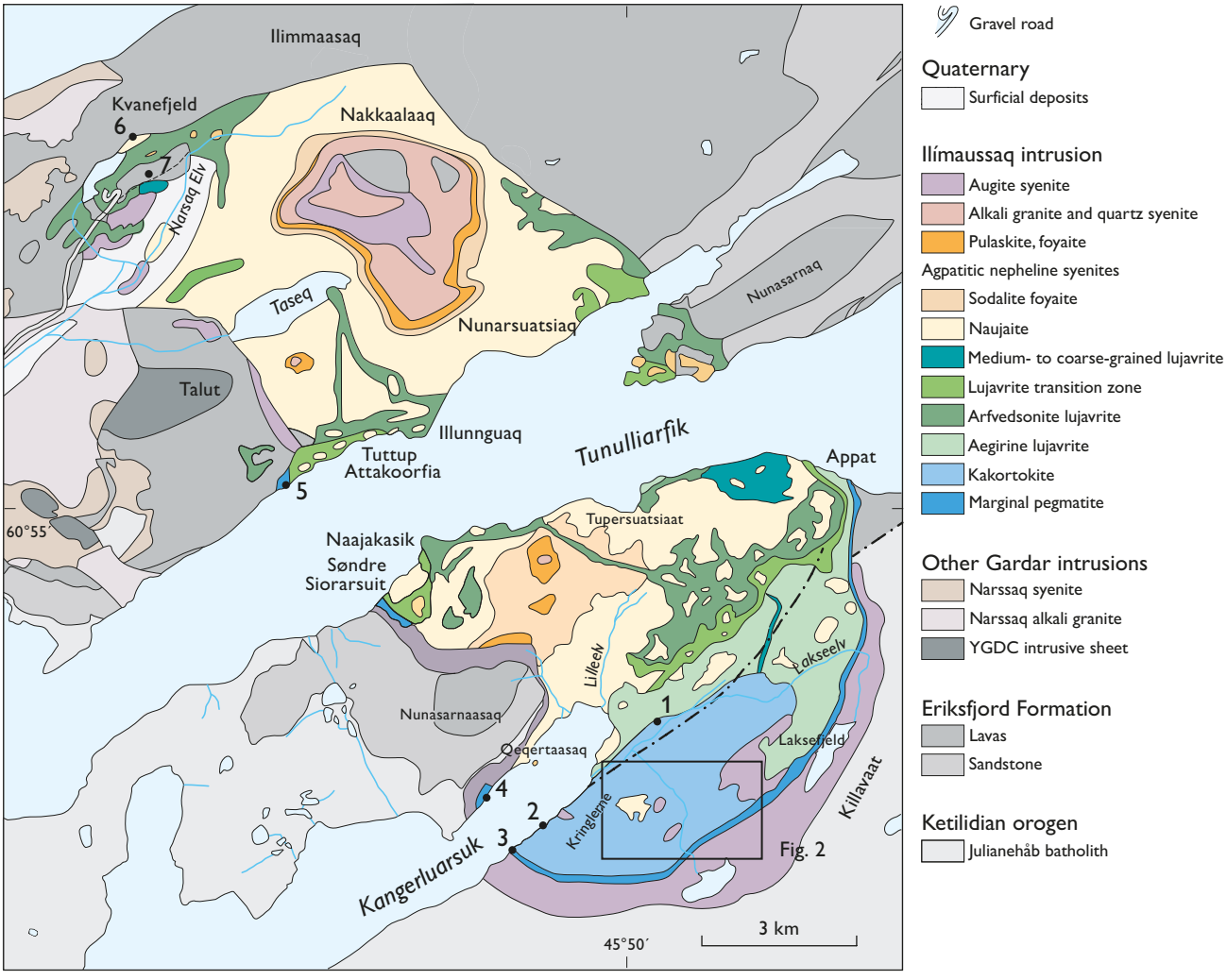

Fig. 1. Simplified geological map of the Ilímaussaq complex based on Ussing (1912), Ferguson (1964) and Andersen *et al*. (1988), redrawn by the Geological Survey of Denmark and Greenland (reproduced with permission). Numbers 1–7 are sample localities outside the area covered by Fig. 2.

and Uk3, and one new Y-rich REE-mineral, Y1, have been identified. The two fergusonite minerals will be treated elsewhere. Mineral A1 has been identified in nearly all eudialyte alteration aggregates from kakortokite, pegmatites and mineral veins, whereas the other alteration minerals occur only in a limited number of samples.

Geological setting of the kakortokite series and associated pegmatites and mineral veins

The Ilímaussaq alkaline complex (Fig. 1) is the type locality of agpaitic nepheline syenites (Ussing 1912). It consists of three main intrusive phases. Phase 1 is a partial rim of undersaturated augite syenite separating the complex from the country rocks. Phase 2 consists of alkali granite and quartz syenite present in the roof zone of the complex. Phase 3 is the main intrusive stage comprising a roof series (from the top and downwards pulaskite, foyaite, sodalite foyaite and naujaite), a floor series (the kakortokites) and in between a series of late lujavrites (e.g. Rose-Hansen & Sørensen 2002; Sørensen 2006; and Sørensen *et al.* 2006). A marginal pegmatite borders the kakortokites in southern Ilímaussaq and is also found at a few localities in the northern part of the complex.

The marginal pegmatite (Ussing 1912; Westergaard 1969; Bohse *at al.* 1971; Karup-Møller *et al.* 2010) consists of agpaitic nepheline syenite and short pegmatitic veins. Within the kakortokite area it has a thickness of about 50 m (Sørensen 1962; Bohse *et al.* 1971; Andersen *et al.* 1988; Karup-Møller *et al.* 2010).

The lower layered kakortokite series (Figs 1 and 2) forms the lowest exposed part of the Ilímaussaq complex (e.g. Ussing 1912; Ferguson 1964; Sørensen 2006; Pfaff *et al.* 2008). It is *c* 200 m thick and consists of a sequence of tri-partite layers each referred to as a unit, and which are repeated at least 28 times. From top to bottom each unit comprises a white layer rich in feldspar and nepheline, a red layer rich in eudialyte, and a black layer rich in arfvedsonite and aegirine. The layering is caused by variation in the modal amounts

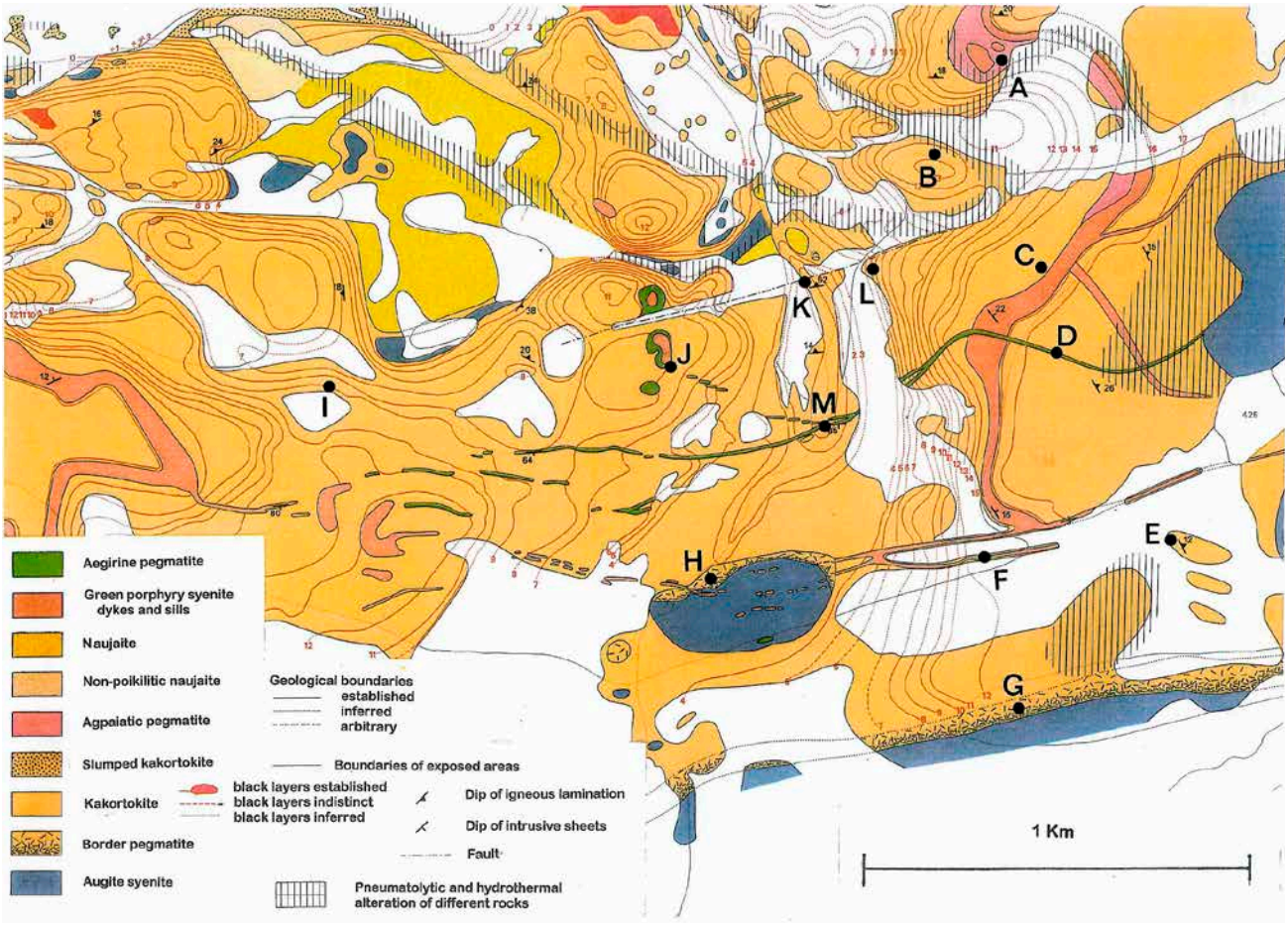

Fig. 2. Geological map of the central part of the kakortokite area, showing sample localities A–M. The map is from Bohse *et al.* (1971) and is reproduced with permission from the Geological Survey of Denmark and Greenland.

of the cumulus minerals. The red and black layers rarely exceed 1 m in thickness. The white layers may reach a thickness of at least 10 m. In the central part of the kakortokite series a distinct unit, named unit 0, has been identified and used as reference level during the mapping of the kakortokite series (Bohse *et al*. 1971). Above this unit, there are 16 units named +1 to +16 in ascending order, and below unit 0 there are 11 units named –1 to –11 in descending order. The lowermost part of the kakortokite is not exposed.

The layered kakortokite series is overlain by *c* 40 m of transitional layered kakortokites in which six eudialyte-rich horizons, named A–F, have been mapped by Bohse *et al*. (1971).

The lujavrites situated between the transitional layered kakortokites and the roof series have a thickness of up to 300 m (Rose-Hansen & Sørensen 2002). They comprise aegirine lujavrite I, aegirine lujavrite II, transitional lujavrite and arfvedsonite lujavrite (Andersen *et al*. 1981; Bohse & Andersen 1981). With decreasing grain size and increasing content of aegirine the transitional layered kakortokites grade into aegirine lujavrite I over a distance of a few metres (Bohse *et al*. 1971). In aegirine lujavrite I there are several eudialyte-rich layers (Henriksen 1993; Bailey 1995), two of which have here been named layer I and II. Layer I is located approximately 5 m from the contact between the transitional layered kakortokites and aegirine lujvrite I and may correspond to layer M1 in drill core 7 logged by Bailey (1995). Eudialyte-rich layer II is located approximately 20 m above layer I. The location is shown in Fig. 1 (loc. 1).

Fig. 3. Agpaitic pegmatite sill at locality A (Fig. 2). The upper 2.5–3.0 m of the sill is distinctly layered. A 10 cm thick grey fine-grained layer (a) in the upper part of the sill separates a more leucocratic lower part from an upper part richer in aegirine and arfvedsonite. Sample 230795 was collected from the grey layer in the pegmatite and samples 151463 and 230797 from the lower part of the pegmatite. Length of hammer handle 43 cm.

Pegmatites and mineral veins

In this work, pegmatites and hydrothermal mineral veins within the kakortokites have been subdivided into three types: agpaitic pegmatites, aegirine pegmatites and oval shaped pegmatites. In addition, there are albititic aplite veins and bodies. The agpaitic pegmatites and several of the largest aegirine pegmatites are shown on the geological map of Bohse *et al*. (1971). The oval-shaped pegmatites and most of the albititic aplites rarely exceed a few metres in size.

The *agpaitic pegmatites* comprise one large sill (Figs 3 and 4) and one vertical dyke. Both are shown on the geological map by Bohse *et al*. (1974). They are mainly

Fig. 4. The upper 1.5 m part of the agpaitic sill shown in Fig. 3, about 100 m east of the location shown in Fig. 3. Here again the grey fine-grained layer (a) separates the sill into a lower leucocratic part (b) and an upper mafic part (c) which is in contact with the overlying trachyte sill (d). A vague layering in the lower and upper parts of the sill is due to slight variations in the proportions of dark and light minerals and grain sizes. Note the two thin layers of coarse material in the fine-grained grey layer. This indicates that the layering of the pegmatite was presumably caused by physical/chemical variations during the crystallization of the sill and is not the result of multiple injections of liquid pegmatitic material.

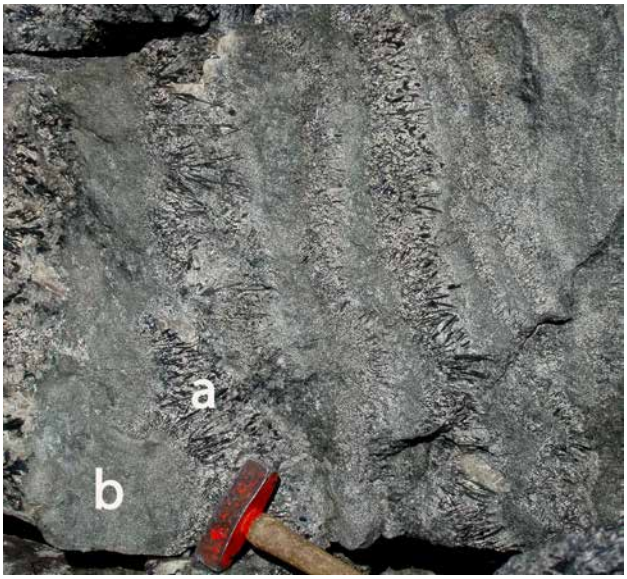

Fig. 5. Aegirine pegmatite in the gully of Laksetværelv (locality M, Fig. 2). Irregular layers of aegirine pegmatitic material (a) alternate with layers of fine-grained green aplitic material (b). The pegmatitic layers are dominated by up to 10 cm long aegirine crystals in poorly shaped rosettes which always grow in the same direction towards east (to the right), indicating that crystallization of the pegmatite took place from west to east.

Fig. 6. Aegirine pegmatite dyke 3 m thick, with marginal zones of very coarse microcline and less coarse central areas (locality B, Fig. 2). Length of hammer handle about 40 cm.

very coarse-grained and dominated by K-feldspar, nepheline and arfvedsonite/aegirine.

The *aegirine pegmatites* vary in thickness from a few centimetres to at least 15 m. They are generally characterized by alternating coarse- and fine-grained, dark green layers which have sharp or gradual contacts against each other (Figs 5 and 6, respectively). The major minerals are feldspar and aegirine.

The *oval-shaped pegmatites* (Figs. 7–9) always occur with sharp contacts against the kakortokite host. Several of these are present at locality I on Fig. 2. The major minerals are K-feldspar, aegirine/arfvedsonite, nepheline and sodalite. Nepheline and sodalite are often partly replaced by analcime.

In addition to the major minerals the pegmatites contain eudialyte (often completely decomposed to secondary minerals) and very small amounts of exotic minerals such as tundrite-(Ce) (Karup-Møller 1982), rinkite, helvite (Johnsen & Bohse 1981), astrophyllite and niobophyllite (Macdonald *et al*. 2007), pectolite, sphalerite, galena, fluorite, native lead and associated secondary litharge and platnerite (Karup-Møller 1975).

Irregularly shaped small *albititic aplites* have either sharp or gradual contacts against the host kakortokite (e.g. at loc. L, Fig. 2). Rarely, albititic aplitic material forms areas within aegirine pegmatites (Fig. 10; loc. J, Fig. 2) and oval-shaped pegmatites (loc. E, F and I, Fig. 2). Albititic aplites also occur as conformable layers in the kakortokite, e.g. at loc. K on Fig. 2. At this locality the aplite layer is about 15 cm thick and can be followed over a distance of about 20 m before disappearing under talus.

Eudialyte and/or eudialyte decomposition products in all pegmatite varieties and in albititic aplites have been included in the present study.

Analytical methods

Electron microprobe analyses were carried out at the Department of Geosciences and Natural Resource Management, University of Copenhagen, using a JEOL 733 superprobe in wavelength dispersive mode with an on-line correction program supplied by JEOL. The accelerating voltage was 15 kV, beam current 15 nA and beam diameter 3 μm. Counting times were 30 seconds on peak positions and 15 seconds on background positions. Wavelengths and standards used were Na *K*α ($NaAlSi_3O_8$), K *K*α ($KAlSi_3O_8$), Ca *K*α and Si *K*α ($CaSiO_3$), Mn *K*α ($MnTiO_3$), Fe *K*α (Fe_2O_3), Al *K*α (Al_2O_3), Ce *L*α (CeO_2), La *L*α (18 wt% La_2O_3 in synthetic glass), Nd *L*α ($Nd_3Ga_5O_{12}$), Pr *L*α ($Pr_3Ga_5O_{12}$), Sm *L*α ($SmFeO_3$), Y *L*α ($Y_3Al_5O_{12}$), Gd *L*α ($GdFeO_3$), Dy, Yb and Er *L*α (all three elements in synthetic silica glass standards), P *L*α and F *K*α (apatite-Wilberforce), Nb *L*α (columbite), Th *M*α (ThO_2), U *M*α (UO_2), and Cl *K*α (sodalite). The estimated detection limit is 0.02 wt% for all elements.

Up to 10 analyses were completed on each phase in a given eudialyte alteration aggregate. All microphotos are back-scattered electron (BSE) images. The analyses of alteration minerals are available in a supplementary data file at the web site http://2dgf.dk/publikationer/bulletin/191bull61.html.

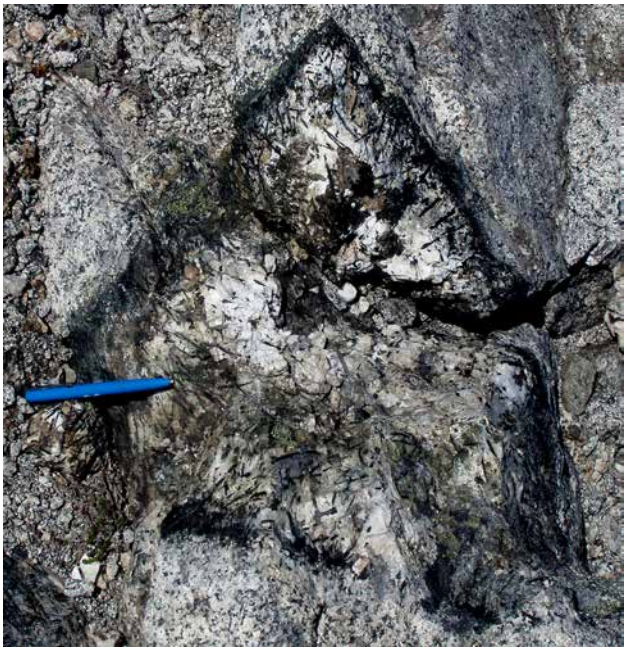

Fig. 7. Small pegmatite geode with high concentrations of aegirine in the border zone against the host kakortokite. The central area is dominated by microcline with minor aegirine and totally decomposed eudialyte (locality I on Fig. 2). About 14 cm ball point pencil for scale.

Fig. 8. Circular pegmatite (a) at locality F with sharp contact against kakortokite (b). The pegmatite is composed of fine-grained aegirine in dense aggregates (1), nepheline (2), microcline (3), eudialyte (4) and arfvedsonite or aegirine (5). Width of photo *c* 60 cm.

Samples studied

Samples with fresh eudialyte and/or totally decomposed eudialyte were taken from the eudialyte-rich red layers in kakortokite units –11, –9, –5, 0, +7, +9, +16, from the eudialyte-rich layers B and D in the transitional layered kakortokite above layer +16, and from the two eudialyte-rich layers I and II in the aegirine lujavrite I. The sample from unit –11 was taken in the white feldspar- and nepheline-rich layer because the red kakortokite layer of this unit was not exposed. Numerous specimens were collected from all three pegmatite types and from albititic aplites. In addition,

Fig. 9. Extremely microcline-rich oval-shaped pegmatite in the kakortokite layer +9 at locality I (Fig. 2). The microcline crystal at the hammer head is more than 30 cm long.

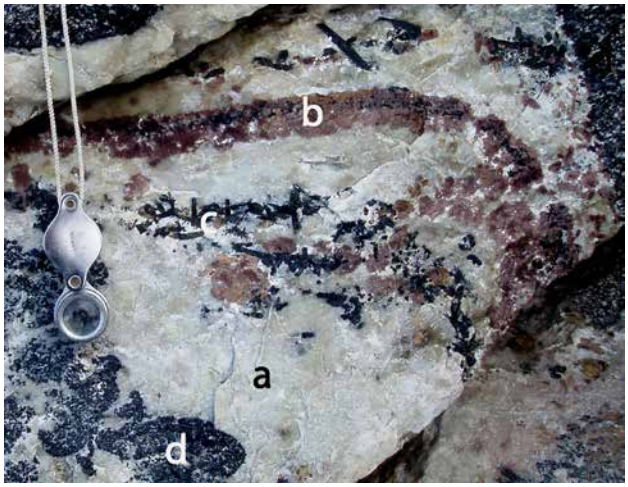

Fig. 10. Fine-grained albititic aplite (a) in the aegirine pegmatite at locality J (Fig. 2), enclosing layered and randomly distributed eudialyte (b) and aegirine (c). Intensely corroded kakortokite remnants (d) are seen in the bottom left part of the photograph. Hand lens 8 cm long.

Table 1. List of investigated layers and samples

Sample	Description	Locality
Layers I, II	Eudialyte-rich layers in green lujavrite	1
Layers A, B, D	Eudialyte-rich layers in transitional kakortokites	1
Layers –11, –9, –5	Eudialyte-rich layers in lower layered kakortokite series	2
Gr2	Marginal pegmatite	3
104361	Marginal pegmatite	4
109302, 109303, 109304	Marginal pegmatite	5
104380	Marginal pegmatite	6
Bore holes 44-22.9 and 48-42.5	Mineralized lujavrites	7
151463; 230790, -91, -95, -96, -97	Agpaitic pegmatite	A
Layer +16	Eudialyte-rich layer in lower layered kakortokite series	A
151460, 230790	Aegirine pegmatite	B
151467	Aegirine pegmatite	C
231301, 231302	Aegirine pegmatite	D
151426, 151428	Circular pegmatite	E
151432	Aplitic phase in circular pegmatite	E
23-1, 23-2, 23-3	Circular pegmatite	F
188188	Marginal pegmatite	G
199195	Marginal pegmatite	H
199199, 199200	Circular pegmatite	I
Layers +7, +9	Eudialyte-rich layer in lower layered kakortokite series	I
151564	Aegirine pegmatite sill	J
Layer 0	Eudialyte-rich layer in lower layered kakortokite series	K
151437	Conformable albititic aplite	K
199176, 199177, 199178	Albititic aplite in kakortokite layer +5	L

Localities 1–7 are shown in Fig. 1 and localities A–L are shown in Fig. 2. The detailed positions of marginal pegmatite and bore holes on Kvanefjeld (Locs 6 and 7) are shown on the geological map of the Kvanefjeld area in Sørensen *et al*. (1974).
All six-digit sample numbers are GGU numbers.

data recorded on mineral A1 from the marginal pegmatite (loc. A–D in Fig. 1 of Karup-Møller *et al*. 2010) have been included in the present study. Monazite from a relatively large number of localities within the kakortokite area (samples 23-2, 23-3, 151428, 199199, layers –9 and –11), the marginal pegmatite (samples 104361, 104380, 199159, 199188) and in drill cores 44-22.9 m and 48-42.5 m from Kvanefjeld, has also been analyzed. All sample localities are shown on Figs 1 and 2 and listed in Table 1.

Mineral descriptions and results

Eudialyte

Analyses of fresh eudialyte were obtained for selected samples from the lujavrite-kakortokite profile, from pegmatitic material at localities E and F, and from albititic aplite at localities E and I (Fig. 2). Small systematic changes in the composition of the mineral were recorded and will be described elsewhere. The average composition of eudialyte in selected samples from the lower layered kakortokite series (units –11, –9, –5, 0, +7, +9, +16) and the transitional layered kakortokites (layers B and D) is listed in Table 3 (no. 1). Following Johnsen & Grice (1999) the analysis has been recalculated on the basis of 29 (Si+Al+Zr+Ti+Nb).

Correlation coefficients for REE in eudialyte are shown in Table 2. All values between 0.1 and –0.1 are considered to be of no significance. Only a weak correlation exists between the elements. Ce is negatively correlated with all the other REE except La. Y is positively correlated with La and Nd but negatively correlated with Pr, Sm and Gd. The weak positive correlation between La and Nd is in sharp contrast to the strong to very strong negative correlation between these two elements in the secondary minerals. The eudialyte analyses are indicated as encircled fields in Fig. 11.

Eudialyte decomposition minerals

Decomposition of eudialyte in the kakortokite series and associated pegmatites and mineral veins has re-

sulted in the formation of catapleiite hosting a number of rare minerals similar to those found in decomposed eudialyte from the marginal pegmatite (Karup-Møller *et al*. 2010). During decomposition, most of the REE in the original eudialyte became concentrated in Ca-rich mineral Al, Ca-poor mineral A1, and some in mineral A2, fergusonite and monazite. Of interest for the study of the minerals A1 and A2 is the distribution of REE in these. Correlation coefficients for REE in A1, A2 and monazite have been calculated.

Table 2. Correlation matrix for REE in eudialyte

	Y	La	Ce	Pr	Nd	Sm	Gd
Y	1.00						
La	0.15	1.00					
Ce	–0.31	0.04	1.00				
Pr	–0.36	–0.30	–0.30	1.00			
Nd	0.44	0.22	–0.18	–0.38	1.00		
Sm	–0.16	–0.22	–0.28	–0.04	–0.10	1.00	
Gd	–0.26	–0.40	–0.29	–0.04	–0.26	–0.09	1.00

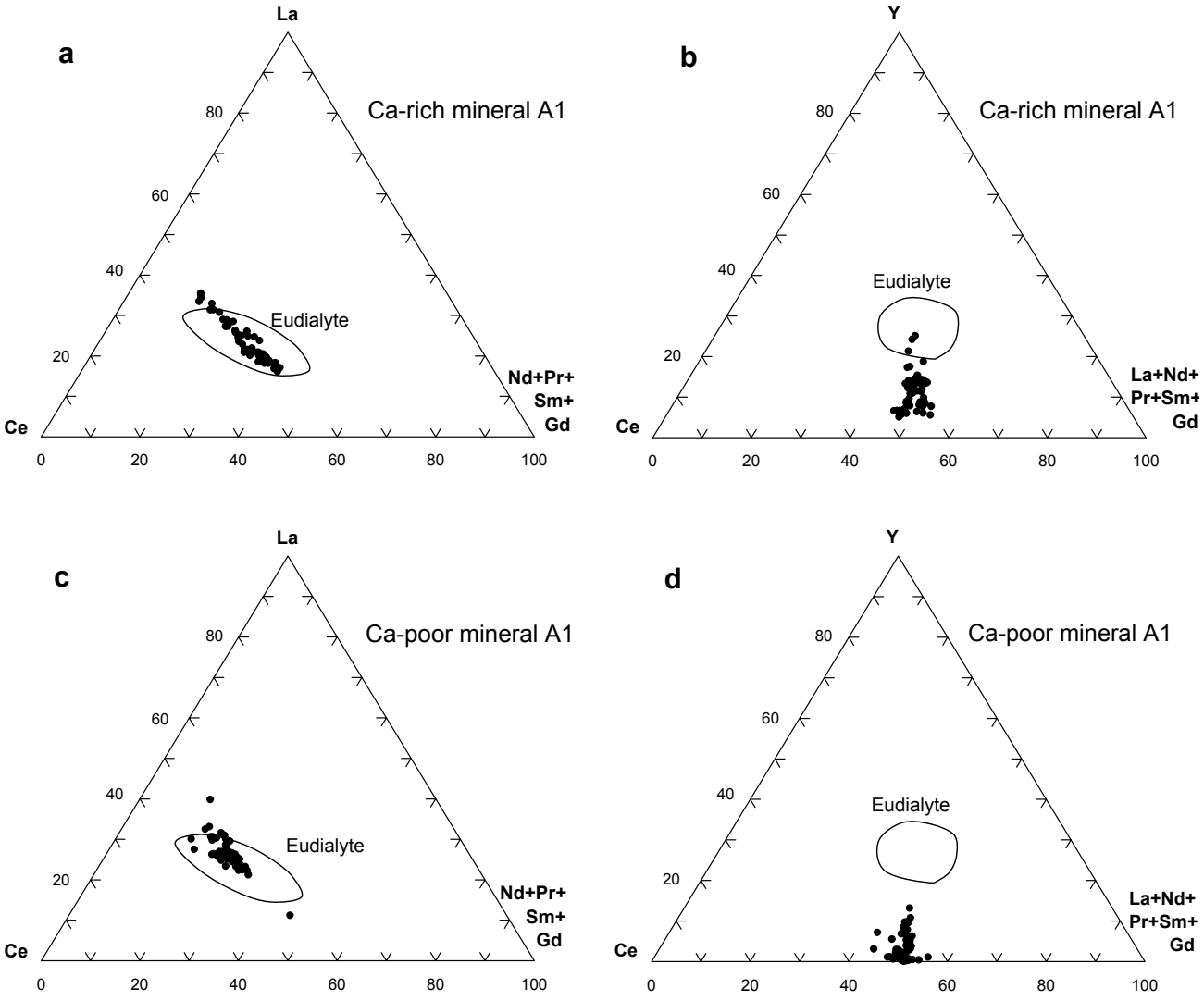

Fig. 11. Molar plots of REE in mineral A1. Analyses of unaltered eudialyte plot within the encircled areas.

Table 3. Microprobe analyses of mineral A1

	1	2	3	4	5	6	7
Mineral	Eudialyte	Ca-rich A1	Ca-poor A1	Ca-poor A1	Altered A1	Altered A1	Ca-poor A1
	Average*	Average	Average	Fig. 16 (c)	Fig. 16 (d)	Fig. 16 (e)	Fig. 17 (c)
No. of analyses	243	106	270	3	3	3	5
SiO_2	49.51 (.36)	22.64 (.57)	23.58 (.59)	19.12 (.07)	21.53 (.50)	18.69 (.67)	20.55 (.52)
TiO_2	0.10 (.01)	-**	-	0.35 (.03)	0.38 (.13)	0.98 (.06)	0.63 (.08)
ZrO_2	11.71 (.15)	0.19 (.48)	0.22 (.29)	-	0.02 (.02)	0.04 (.04)	0.07 (.05)
ThO_2	-	0.11 (.09)	0.22 (.28)	0.20 (.14)	4.99 (.98)	8.23 (.70)	5.83 (.87)
P_2O_5	-	0.81 (.45)	0.44 (.01)	6.00 (.64)	1.28 (.16)	0.81 (.17)	1.18 (.15)
Al_2O_3	0.25 (.02)	-	0.18 (.18)	0.08 (.03)	0.35 (.01)	1.77 (.04)	0.78 (.07)
Nb_2O_5	0.76 (.13)	-	-	0.27 (.12)	1.30 (.59)	6.61 (.66)	3.95 (.60)
Y_2O_3	0.46 (.05)	4.02 (2.00)	1.18 (1.26)	0.36 (.06)	0.70 (.26)	3.04 (.19)	2.38 (.33)
La_2O_3	0.48 (.03)	12.81 (3.34)	16.67 (2.67)	19.63 (.69)	11.87 (.76)	11.07 (.60)	13.41 (1.05)
Ce_2O_3	0.97 (.07)	26.78 (2.30)	31.66 (2.10)	32.33	29.82 (.42)	25.33 (.74)	27.67 (.65)
Pr_2O_3	0.13 (.02)	2.54 (.43)	2.71 (.43)	2.46 (.30)	2.49 (.27)	1.88 (.34)	2.39 (.35)
Nd_2O_3	0.39 (.04)	11.64 (2.43)	10.99 (1.99)	9.69 (.49)	11.66 (.85)	7.66 (.56)	8.96 (.52)
Sm_2O_3	0.11 (.02)	2.75 (1.00)	1.98 (.68)	1.56 (.36)	1.99 (.35)	1.36 (.27)	1.61 (.23)
Gd_2O_3	0.10 (.04)	1.86 (.80)	0.89 (.59)	0.27 (.07)	0.64 (.16)	0.90 (.12)	0.87 (.26)
FeO	6.10 (.27)	0.13 (.31)	2.01 (.69)	1.19 (.04)	1.25 (.19)	0.96 (.12)	1.22 (.07)
MnO	0.68 (.05)	0.00	0.45 (.49)	1.35 (.08)	1.15 (.05)	2.71 (.23)	1.22 (.29)
CaO	9.89 (.58)	11.07 (.69)	2.90 (.90)	0.78 (.12)	1.97 (.21)	1.61 (.10)	1.94 (.06)
K_2O	0.28 (.06)	-	-	-	0.04 (.01)	0.04 (.04)	0.05 (.01)
Na_2O	14.53 (.54)	0.00	0.26 (.37)	2.63 (.26)	0.32 (.03)	0.04 (.04)	0.28 (.06)
F	0.05 (.02)	1.34 (.15)	1.01 (.26)	1.08 (.04)	1.18 (.06)	0.86 (.07)	1.16 (.07)
Cl	1.40 (.14)	-	-	-	-	-	-
F,Cl–O corr.	–0.34	–0.56	–0.43	–0.45	–0.50	–0.36	–0.49
Total	97.56	98.13	96.92	98.90	94.43	94.23	95.66
Atoms based on Si+Zr+P = 6.00**							
Si	25.68	5.80	5.89	4.74	5.71	5.78	5.80
Ti	0.03	-	-	0.06	0.08	0.23	0.13
Zr	2.96	0.02	0.04	-	-	0.01	0.01
Th	-	0.01	0.01	0.01	0.30	0.58	0.38
P	-	0.18	0.07	1.26	0.29	0.21	0.19
Al	0.15	-	0.05	0.02	0.11	0.65	0.39
Nb	0.18	-	-	0.03	0.16	0.93	0.51
Y	0.13	0.55	0.16	0.05	0.10	0.50	0.36
La	0.09	1.21	1.54	1.80	1.16	1.27	1.40
Ce	0.18	2.52	2.90	2.94	2.90	2.87	2.87
Pr	0.03	0.24	0.25	0.22	0.24	0.21	0.25
Nd	0.07	1.07	0.98	0.86	1.11	0.85	0.91
Sm	0.01	0.24	0.17	0.13	0.18	0.15	0.16
Gd	0.01	0.15	0.07	0.02	0.06	0.09	0.08
ΣREE	0.53	5.98	6.07	6.02	5.75	5.94	6.03
Fe	2.66	0.03	0.42	0.25	0.28	0.25	0.29
Mn	0.30	-	0.09	0.28	0.26	0.71	0.29
Ca	5.50	3.04	0.78	0.21	0.56	0.53	0.59
K	0.18	-	-	-	0.01	0.01	0.02
Na	14.62	-	0.13	1.27	0.16	0.03	0.15
F	0.09	1.08	0.80	0.85	0.99	0.84	1.03
Cl	1.23						

* - = below detection limit Numbers in parentheses are 1σ

** The eudialyte recalculation is based on 29 (Si+Ti+Zr+Al+Nb)

1: Average of eudialyte from the kakortokite series. 2: Average of all Ca-rich mineral A1 analyses. 3: Average of all Ca-poor mineral A1 analyses. 4–7: Analyses of fresh and altered Ca-poor mineral A1 in sample 23-2 (circular pegmatite).

Mineral A1

Mineral A1 appears occasionally as individual lath-shaped crystals in random distribution throughout eudialyte alteration aggregates, but it is mostly found in clusters of crystals (Figs 12 and 13).

Karup-Møller *et al*. (2010, their Table 2) found the average composition of A1 in eudialyte decomposition aggregates from the marginal pegmatite to be $(Na,Ca,Fe,Mn)_2Ce_3REE_3Si_6FO_{22.5}$. However, additional microprobe analyses on this mineral in altered eudialyte from the kakortokite area have proved the existence of two varieties, a Ca–rich A1 and a Ca-poor A1. Continuous solid solution between these two varieties does not appear to exist. In Fig. 14 both phases show sharp contacts to each other, confirming this conclusion. They have therefore been treated separately.

The major chemical difference between Ca-rich and Ca-poor mineral A1, apart from their Ca contents, is the presence of small contents of Fe, Mn and Na in Ca-poor A1. Mn and Na have not been detected in Ca-rich A1 and the average content of Fe in this mineral is less than 0.1 wt%. The proportions between the REE in the two A1 varieties are rather similar (Table 3). The most noteworthy difference is the higher contents of Ce and La and the lower contents of Y in Ca-poor A1 compared to Ca-rich A1.

A pronounced variation in the content of individual REE, in particular La and Nd, exists for both mineral varieties from grain to grain in individual decomposition aggregates. In order to determine the substitutional relationships between the elements, correlation matrices (Tables 4 and 5) and triangular plots for certain elements and element combinations (Fig. 11) were completed on all A1 analyses, leading to the average values in Table 3 (nos 2–3). The results of the substitutional relationships are reported below.

Ca-rich mineral A1

The average composition of a total of 106 individual analyses of Ca-rich A1 is listed in Table 3 (no. 2). Characteristic for all analyses is a molar ratio of Si (+Zr+P) to REE close to 1:1. Only limited analyses for the HREE Dy, Yb and Er were completed on Ca-rich A1 in sample 230795 (see the supplementary data file).

From the correlation matrix in Table 4 it is seen that Ca is negatively correlated with Ce, Y and La but positively correlated with Nd, Pr, Sm and Gd. Cerium is also negatively correlated with these four elements and Y, but positively correlated with La. There is a strong positive correlation internally between Nd, Pr, Sm and Gd. These relationships can to some extent also be read from Fig. 11a. Here a linear relationship shows that a decreasing content of Pr+Nd+Sm+Gd is accompanied by an increasing content of La and

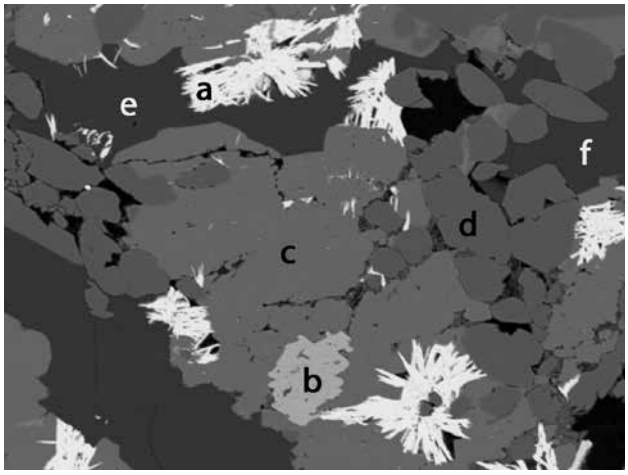

Fig. 12. Eudialyte decomposition aggregate composed of Ca-poor mineral A1 (a), zircon (b), catapleiite (c), aegirine (d), possibly analcime (e), and K-feldspar (f). Sample 231301. Width of image 0.26 mm.

Fig. 13. Cluster of lath-shaped mineral A1 crystals isolated in K-feldspar. Kakortokite layer 0. Width of image 0.07 mm.

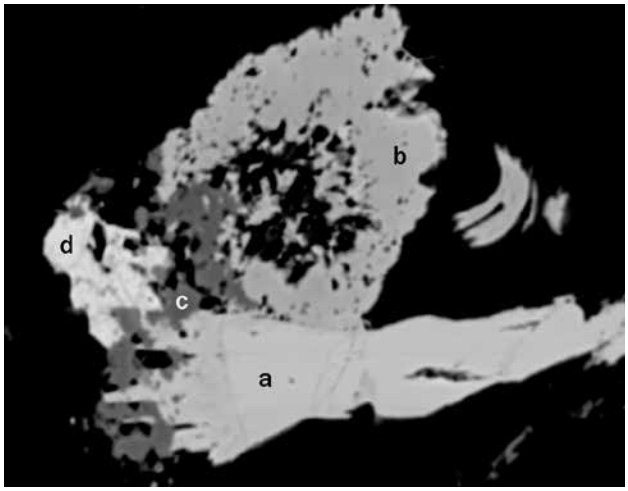

Fig. 14. Aggregate composed of Ca-poor A1 (a), Ca-rich A1 (b), an unidentified Nb-mineral (c) and fergusonite (d). Sample 151437, albititic aplite. Width of image 0.06 mm.

Table 4. Correlation matrix for elements in Ca-rich mineral A1

	Ca	Y	La	Ce	Pr	Nd	Sm	Gd
Ca	1.00							
Y	–0.11	1.00						
La	–0.47	–0.18	1.00					
Ce	–0.53	–0.61	0.75	1.00				
Pr	0.04	–0.27	–0.47	–0.14	1.00			
Nd	0.22	–0.28	–0.83	–0.33	0.66	1.00		
Sm	0.36	–0.14	–0.87	–0.53	0.56	0.91	1.00	
Gd	0.53	0.10	–0.84	–0.76	0.40	0.68	0.78	1.00

a moderate increase in the content of Ce. Finally Y displays a weak negative correlation with La, Pr, Nd and Sm, but a very weak positive correlation with Gd. The small plot area in Fig. 11b confirms these poorly defined relationships. Calcium follows Pr, Nd, Sm and Gd but has not been included in the plot.

Ca-poor mineral A1

The average composition of 270 analyses of Ca-poor A1 is listed in Table 3 (no. 3). As for the Ca-rich A1, the molar ratio of Si (+Zr+P) to REE is close to 1:1. The correlation matrix for Ca-poor A1 (Table 5) is, with a few exceptions, similar to that for Ca-rich A1. It is seen that Fe is positively correlated with Ca. A major difference between the two matrices is the positive correlation between Ca and Pr, Nd, Sm and Gd in Ca-rich A1 and the negative correlation between these elements in Ca-poor A1. In Fig. 11c the analyses cluster in a slightly oval-shaped area in rather sharp contrast to the linear relationships recorded for Ca-rich A1 (compare Fig. 11a with 11c). The plots in Figs 11b and 11d are similar; the only difference is higher contents of Y in Ca-rich A1 than in Ca-poor A1.

Nb-bearing Ca-poor mineral A1

Ca-poor A1 with small amounts of Nb and Th was found in sample 23-3 from the small and poorly exposed pegmatite at locality F in Fig. 2. It occurs within cavities in aegirine after an unknown mineral, probably villiaumite (NaF), and the following minerals were formed: catapleiite, Ca-poor A1, monazite, an unidentified Nb-mineral, thorite, and poorly defined Mn-hydroxides or carbonates.

Catapleiite is the dominant mineral in the aggregate shown in Fig. 15. The mineral occurs as thin laths forming a pseudohexagonal open intergrowth. Cavities are partly filled with the unidentified Nb-mineral. Enclosed between the catapleiite laths there are a few relatively large and almost completely decomposed Ca-poor A1 crystals. The most centrally placed of these is shown in Fig. 16 where the different REE-minerals can be distinguished. The precipitation of the Nb-mineral in cavities between catapleiite crystals is accompanied by its crystallization along fractures. Presumably at the same time almost complete replacement of the original A1 (Table 3 no. 4) took place. Two stages in this replacement process can be recognized in Fig. 16. In the lower left part of the picture the two A1-like replacement phases (d and e) can be recognized. Analyses of these two phases are listed in Table 3, nos 5 and 6. As a result of this replacement process, Na was almost completely removed from the primary A1 and the content of P was strongly reduced. The content of Nb, Th and Al was increased from close to nil in A1 to substantial amounts in the phase at point e in Fig. 16. The total content of REE was not signifi-

Table 5. Correlation matrix for elements in Ca-poor mineral A1

	Ca	Fe	Y	La	Ce	Pr	Nd	Sm	Gd
Ca	1.00								
Fe	0.15	1.00							
Y	0.36	0.15	1.00						
La	–0.18	–0.14	–0.58	1.00					
Ce	–0.66	–0.31	–0.80	0.57	1.00				
Pr	–0.41	–0.13	–0.24	0.36	0.42	1.00			
Nd	–0.33	–0.06	–0.08	–0.67	–0.10	0.66	1.00		
Sm	–0.06	0.01	–0.43	0.31	–0.73	0.71	0.34	1.00	
Gd	0.10	–0.25	–0.30	0.11	–0.38	–0.38	0.15	0.56	1.00

cantly changed as a result of this alteration process, but the REE distribution changed. A decrease in the element oxide sum from 99.35 wt% in the primary A1 to 94.59 wt% in the most replaced variety (Table 3 no. 6) suggests that hydration (or carbonatization) accompanied the replacement process.

Figure 17 shows crystals of catapleiite that have grown from the walls of an empty space. A group of Nb-bearing A1 lamellae (composition in Table 3 no. 7) occurs in the bottom right part of the picture. The mineralization was terminated by the precipitation of a thin crust of the Nb-mineral upon the catapleiite crystals, sometimes filling cavities between these as seen in Figs 15 and 16. The composition of the Nb-bearing A1 lamellae resembles the composition of the Nb-bearing last phase in the replacement process after

Fig. 15. Cavity in aegirine (a) filled with lamellar catapleiite (b) which encloses strongly altered Ca-poor A1 crystals (c). Cavities between the catapleiite crystals (d) are partly filled with an unidentified Nb-bearing mineral (e). It is not possible to distinguish between A1 and the Nb-mineral in the picture. Therefore the lower central part of the area, covering most of the A1 crystals, is shown at a lower electron flux in Fig. 16. Sample 23-2, circular pegmatite. Width of image 0.46 mm.

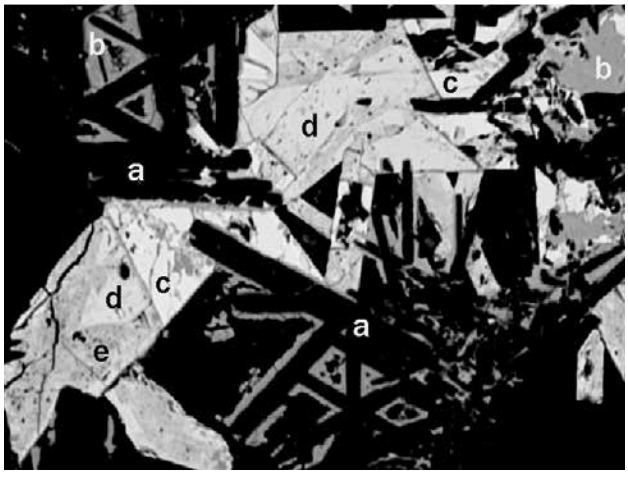

Fig. 16. The lower central area in Fig. 15 recorded at low electron flux which has resulted in easy distinction between the various phases present. Catapleiite (a) is encrusted by a thin layer of an unidentified Nb-mineral (b); sometimes cavities are completely filled with this mineral. The majority of early precipitated A1 (c) has been altered. Two stages (d) and (e) in this alteration process can be recognized. Width of image 0.21 mm.

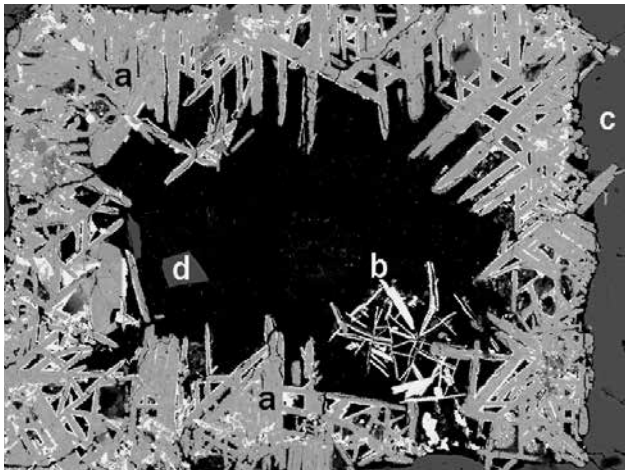

Fig. 17. Cavity in aegirine close to the cavity shown in Figs 15 and 16, partly filled with catapleiite crystals (a), Ca-poor A1 (b) and an unidentified Nb-mineral encrusting catapleiite crystals and partly filling cavities between these (c). The central black area with a crystal of aegirine (d) is epoxy-filled empty space. Sample 23-2, circular pegmatite. Width of image 0.70 mm.

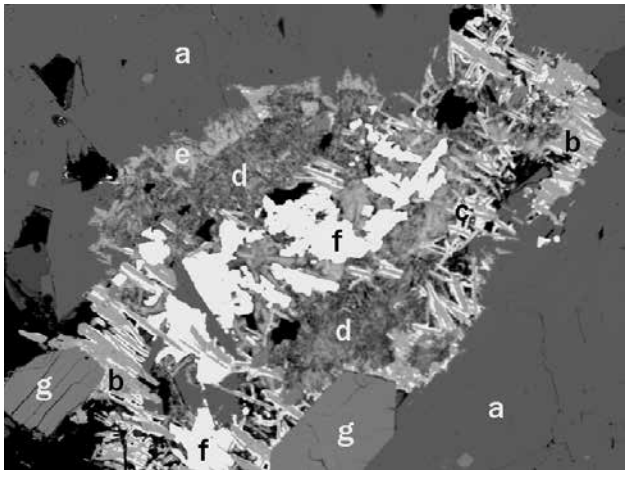

Fig. 18. Cavity in K-feldspar (a) filled with catapleiite (b) encrusted by an unidentified Nb-mineral (c, grey-white), and two Mn-hydroxides and/or carbonates (d, e) enclosing an aggregate (f) of monazite and thorite indistinguishable from each other on the figure. Aegirine crystals (g) are also present. Sample 23-2, circular pegmatite. Width of image 1.64 mm.

mineral A1 in Fig. 16. A similar replacement process may also have taken place here (Fig. 17) but cannot be recognized due to the small size of the lamellae.

In another mineral aggregate in the same sample (Fig. 18), we have identified a heterogeneous mixture of catapleiite, the unidentified Nb-mineral, two Mn-hydroxides or carbonates, monazite and thorite.

Mineral A2

In contrast to mineral A1, mineral A2 was only found at a limited number of pegmatite localities within the kakortokite area. Like A1, it occurs as a secondary mineral in eudialyte decomposition aggregates. In backscattered images in the microprobe it is not possible to distinguish between the two minerals. Mineral A2 was originally found in sample 104361 from the marginal pegmatite (Loc. 4, Fig. 1) (Karup-Møller *et al*. 2010). In one sample mineral A2 was also found as a primary mineral (Fig. 19). In another sample a phase close in composition to A2 was identified (Fig. 20). The compositions of all the phases mentioned are listed in Table 6.

Mineral A2 has a molar ratio of Si:REE close to 3:2. It has no detectable contents of Zr, Ti, Th, Al, P or F. A2 is relatively rich in Y and to some extent also Gd compared to A1. This would imply that the mineral also contains relatively high amounts of HREE, but as seen from Table 6 this is not the case. The low element oxide sum obtained therefore cannot be explained by missing HREE but indicates that A2 is a hydrous or carbonate-bearing mineral . The analyses of A2 in the eudialyte decomposition aggregates show that there is a large difference in composition from grain to grain within the same sample (and often also from grain to grain within individual decomposition aggregates). In order to illustrate the substitutional relationships between the elements in A2, correlation coefficients and element plots similar to those carried out for mineral A1 are presented.

From the correlation matrix in Table 7 it is seen that both Ca and Fe are positively correlated with La and negatively correlated with the other REE. Thus grains relatively rich in La contain relatively more Fe and Ca than those poorer in La. There is no correlation between Y and Ca and only a weak positive correlation between Y and Fe. Furthermore, La is positively correlated with Ce and negatively correlated with Pr, Nd, Sm and Gd. This is also evident from the triangular Ce-La-(Pr+Nd+Sm+Gd) plot in Fig. 21a. Table 7 shows that Y is negatively correlated with the other REE. This is also seen from the plot Ce-Y-(La+Pr+Nd+Sm+Gd) in Fig. 21b. Here the A2 plot covers a rather broad range and overall increasing contents of Y are accompanied by decreasing contents of all other REE.

The original formula for A2 from the marginal pegmatite (Karup-Møller *et al*. 2010) was proposed as $REE_3Si_4O_{12.5-y}(OH)_{2y} \cdot nH_2O$, ignoring the small amounts of Fe and Ca recorded. On the basis of the average A2 analyses in Table 6 no. 1, the following simplified empirical formula for A2 is here proposed: $(Ca,Fe)_{1.2}REE_4Si_6O_{19.2-y}(OH)_{2y} \cdot nH_2O$.

In sample 231301, mineral A2 was found as a primary mineral enclosed in a fine-grained homogeneous intergrowth of aegirine and analcime. The sample represents the fine-grained albite phase of the large aegirine pegmatite at locality D, Fig. 2. Here the A2 grains are relatively large (Fig. 19) and all delicately zoned. The lightest zones have a composition close to that of A2 in the eudialyte decomposition aggregates (Table 6 no. 2). The darkest zones have a high content

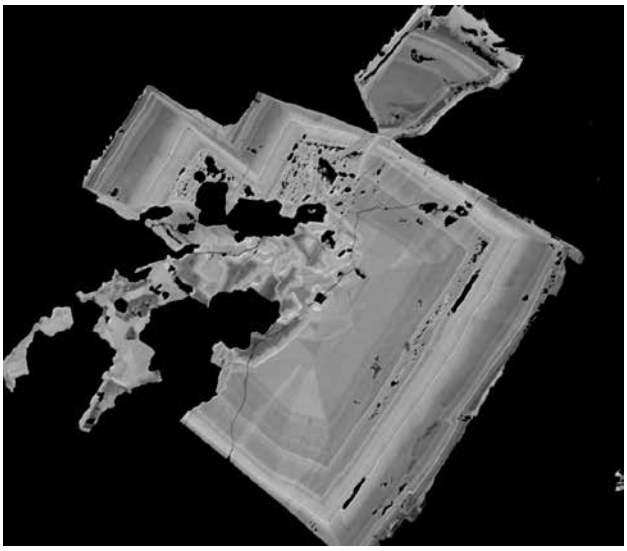

Fig. 19. Primary mineral A2 grain showing zoning. Sample 231301, aegirine pegmatite. Width of image 0.21 mm.

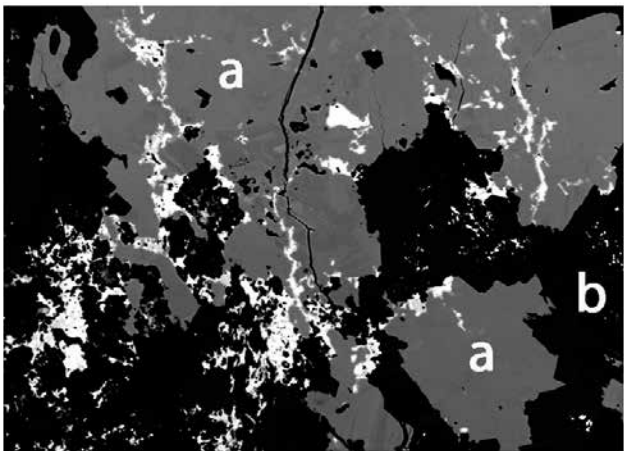

Fig. 20. Irregular veinlets and patches of mineral A2-like phase (white) in zircon (a) and K-feldspar (b) in a eudialyte decomposition aggregate. Sample 151460, aegirine pegmatite. Width of image 0.29 mm.

of Y and correspondingly lower content of the other REE, particularly Ce and Nd (Table 6 no. 3). A gradual change in composition of the mineral from light to dark zones is assumed to exist. The compositional range of mineral A2 is thus defined by, at the one end, the darkest zones in the A2 grains in sample 231301 with maximum content of Y and corresponding low contents of the other REE, and, at the other end, by A2 grains in eudialyte decomposition aggregates with minimum content of Y and correspondingly high contents of the other REE.

A mineral close in composition to A2 was found in sample 151460. The mineral occurs as irregularly shaped veinlets grading into clusters of disseminated grains in zircon and K-feldspar (Fig. 20). The proportions between the individual REE in A2 and in this mineral variety are strikingly different (Table 6 no. 4) but the Si:REE ratio of 6:4.47 is close to that of ideal A2.

Table 6. Microprobe analyses of mineral A2

	1	2	3	4	5
	Av. secondary	Primary, light	Primary, dark	Secondary	Secondary
No of analyses	82	2	3	9	7
SiO_2	27.38 (1.17)	29.92 (.26)	30.23 (.21)	27.60 (.55)	26.90 (.24)
Y_2O_3	7.31 (3.73)	2.74 (.09)	19.51 (.43)	2.12 (.60)	2.44 (.73)
La_2O_3	5.72 (1.78)	5.35 (.11)	2.63 (.02)	13.29 (2.18)	1.91 (.32)
Ce_2O_3	17.73 (2.81)	18.29 (.27)	8.23 (.37)	27.04 (.74)	16.41 (1.38)
Pr_2O_3	2.16 (.64)	2.55 (.34)	1.37 (.26)	2.27 (.40)	3.20 (.43)
Nd_2O_3	11.19 (2.58)	14.86 (.09)	6.32 (.13)	8.65 (1.00)	19.30 (.92)
Sm_2O_3	3.16 (1.08)	3.62 (.30)	1.70 (.18)	1.39 (.45)	6.36 (.41)
Gd_2O_3	2.40 (1.34)	3.65 (.52)	3.11 (.13)	0.75 (.31)	4.38 (.55)
Dy_2O_3	n.a.**	0.88 (.01)	2.81 (.56)	n.a.	n.a.
Er_2O_3	n.a.	-*	0.64 (.12)	n.a.	n.a.
Yb_2O_3	n.a.	-	0.61 (.28)	n.a.	n.a.
FeO	2.22 (1.33)	3.80 (.08)	3.69 (.13)	0.69 (.35)	-
CaO	3.39 (1.58)	4.22 (.01)	5.81 (.17)	2.82 (.29)	1.21 (1.3)
Na_2O	-	0.53 (.01)	-	-	-
F	-	-	-	-	0.22 (.15)
F–O corr.	-	-	-	-	–0.09
Total	82.66	90.41	86.66	86.62	82.24
Atoms based on Si = 6.00					
Si	6.00	6.00	6.00	6.00	6.00
Y	0.85	0.29	2.06	0.25	0.29
La	0.46	0.40	0.19	1.07	0.16
Ce	1.42	1.34	0.60	2.16	1.34
Pr	0.17	0.19	0.10	0.18	0.26
Nd	0.88	1.07	0.45	0.67	1.55
Sm	0.24	0.25	0.12	0.10	0.50
Gd	0.17	0.24	0.20	0.05	0.32
Dy		0.04	0.18		
Er		-	0.04		
Yb		-	0.04		
∑REE	4.19	3.82	3.98	4.48	4.42
Fe	0.41	0.43	0.61	0.12	-
Ca	0.80	0.61	1.23	0.66	0.29
Na	-	0.21	-	-	-
F	-	-	-	-	0.29

* - = below detection limit ** n.a. = not analysed Numbers in parentheses are 1σ

1: Average of mineral A2 grains in eudialyte decomposition aggregates. 2 and 3: zones in primary A2 grain in sample 230301 (Fig. 19) from aegirine pegmatite. 4: Phase resembling A2 in sample 151460 (Fig. 20) from aegirine pegmatite. 5: mineral A2 in decomposed eudialyte in sample 104361 from the marginal pegmatite.

Table 7 Correlation matrix for elements in mineral A2

	Ca	Fe	Y	La	Ce	Pr	Nd	Sm	Gd
Ca	1.00								
Fe	0.73	1.00							
Y	–0.05	0.21	1.00						
La	0.24	0.29	–0.51	1.00					
Ce	–0.40	–0.54	–0.82	–0.51	1.00				
Pr	–0.59	–0.58	–0.42	–0.06	0.56	1.00			
Nd	–0.81	–0.85	–0.37	–0.30	0.59	0.69	1.00		
Sm	–0.78	–0.87	–0.17	–0.48	–0.40	0.58	0.92	1.00	
Gd	–0.63	–0.82	–0.13	–0.48	–0.28	0.46	0.75	0.81	1.00

Mineral A2 in sample 104361, from the marginal pegmatite, has a Si:REE ratio of 6:4.42 (Table 6 no. 5) which is similar to that of A2 from the kakortokites. The proportions between the REE in A2 from the two areas are also comparable.

Monazite

Monazite occurs in decomposed eudialyte as isolated apparently primary grains in silicate minerals and as a decomposition mineral after an unknown mineral. The average chemical composition of the mineral, excluding analyses from samples 23-2 and 199195, is listed in Table 8 no. 1 and results in the formula: $(Ce_{0.48}La_{0.30}Pr_{0.04}Nd_{0.12}Sm_{0.01}Ca_{0.01})_{\Sigma 0.96}(P_{0.97}Si_{0.03})_{\Sigma 1.00}F_{0.03}O_{3.90}$. From the correlation coefficients for monazite (Table 9), it is seen that Ce is negatively correlated with La and Y and positively correlated with Nd, Pr and Sm. La is negatively correlated with Nd, Pr, Sm and Gd. This is also seen from the Ce-La-(Pr+Nd+Sm+Gd) plot in Fig. 22, which displays the same general trend as that recorded for both Ca-rich and Ca-poor A1.

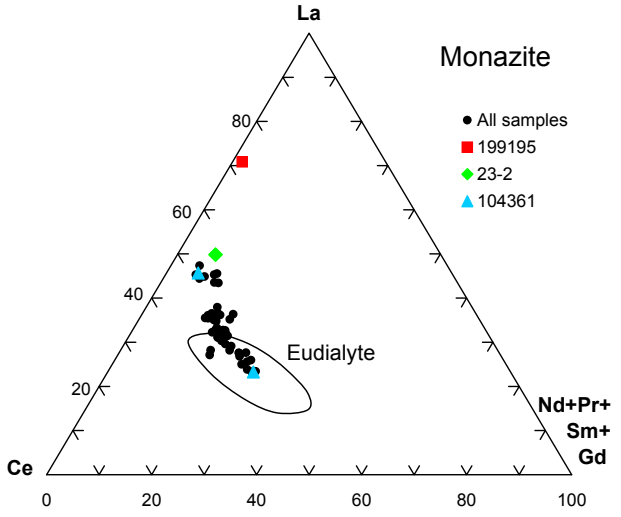

Fig. 22. Molar plot of REE in monazite. "All samples" exclude the two samples 199195 and 23-2 plotted separately. The two analyses from 104361 plotted separately are the extremes given in Table 8. Analyses of unaltered eudialyte plot within the encircled area. See text for discussion.

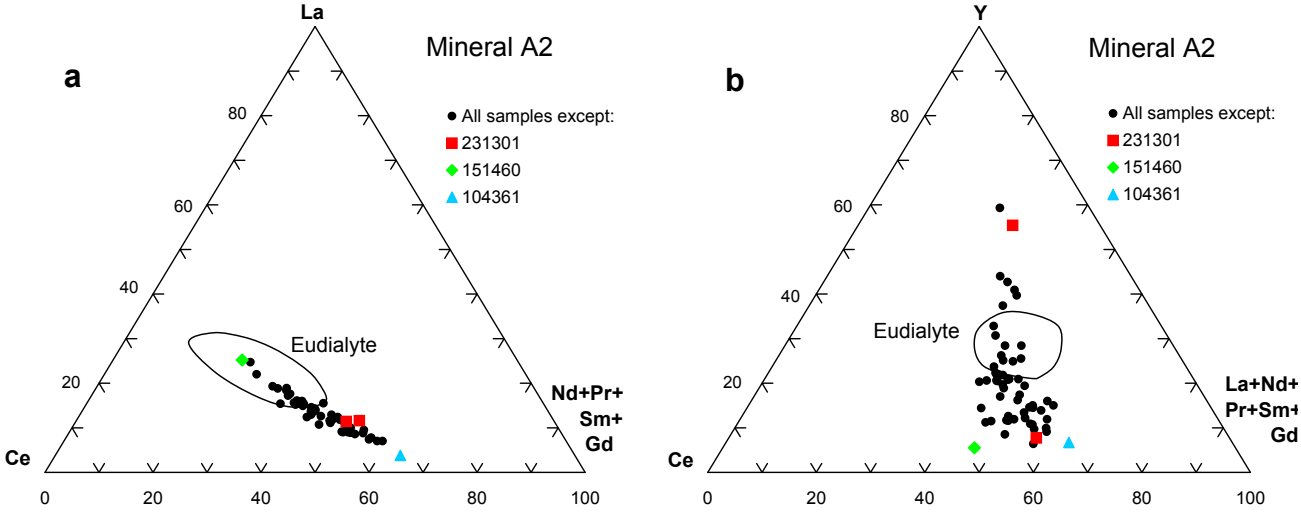

Fig. 21. Molar plots of REE in mineral A2. Analyses of unaltered eudialyte plot within the encircled areas. See text for discussion.

Table 8. Microprobe analyses of monazite

	1	2	3	4	5
Sample no.	All analyses*	104361 lightest	104361 darkest	23-2	199195
No. of analyses	134	3	3	13	4
SiO_2	0.84 (.84)	0.67 (.02)	0.08 (.03)	0.29 (.25)	0.44 (.41)
TiO_2	0.02 (.03)	-	-	0.03 (.03)	-
ZrO_2	0.09 (.18)	0.05 (.04)	-	0.04 (.05)	-
ThO_2	0.38 (.53)	0.48 (.05)	-	0.22 (.20)	0.43 (.42)
UO_2	0.02 (.01)	n.a.**	n.a.	0.02 (.01)	0.06 (.07)
P_2O_5	30.86 (1.20)	31.53 (.26)	31.88 (.63)	31.75 (.69)	31.44 (.96)
Al_2O_3	0.03 (.07)	-	-	0.02 (.02)	-
Nb_2O_3	0.03 (.03)	-	-	0.04 (.08)	-
Y_2O_3	0.04 (.05)	0.06 (.05)	-	0.05 (.06)	0.04 (.04)
La_2O_3	21.95 (3.90)	16.04 (.23)	32.28 (1.07)	35.59 (3.25)	49.43 (1.56)
Ce_2O_3	35.09 (1.56)	34.01 (.26)	34.36 (.64)	30.88 (1.89)	19.19 (.90)
Pr_2O_3	2.62 (.58)	3.33 (.25)	1.30 (.15)	1.35 (.34)	0.44 (.16)
Nd_2O_3	8.80 (2.59)	13.59 (.41)	2.65 (.25)	3.74 (1.16)	0.73 (.10)
Sm_2O_3	0.89 (.53)	2.02 (.14)	0.39 (.13)	0.17 (.20)	-
Gd_2O_3	0.20 (.23)	0.87 (.29)	0.05 (.09)	0.07 (.06)	0.14 (.17)
FeO	0.02 (.02)	-	-	-	0.05 (.06)
MnO	0.02 (.03)	-	-	-	0.05 (.07)
CaO	0.17 (.28)	0.04 (.01)	0.02 (.02)	0.03 (.02)	0.03 (.03)
K_2O	0.02 (.03)	-	-	-	0.04 (.04)
Na_2O	0.02 (.06)	-	-	-	-
F	0.22 (.26)	0.05 (.02)	0.04 (.03)	0.37 (.23)	0.42 (.17)
F–O corr.	–0.09	–0.02	–0.02	–0.16	–0.18
Total	102.24	102.72	103.03	104.50	102.75
Atoms based on P+Si = 10.00					
Si	0.31	0.24	0.03	0.11	0.16
Ti	-	-	-	-	-
Zr	0.02	0.02	-	-	-
Th	0.03	-	-	0.02	0.04
U	-	-	-	-	-
P	9.69	9.76	9.97	9.89	9.84
Al	0.01	-	-	-	-
Nb	-	-	-	-	-
Y	-	0.01	-	0.01	-
La	3.00	2.16	4.40	4.83	6.79
Ce	4.76	4.55	4.65	4.16	2.60
Pr	0.35	0.44	0.18	0.18	0.06
Nd	1.16	1.78	0.35	0.49	0.10
Sm	0.11	0.26	0.05	0.02	-
Gd	0.02	0.11	-	-	0.02
∑REE	9.40	9.31	9.63	9.69	9.57
Fe	-	-	-	-	0.01
Mn	-	-	-	-	0.01
Ca	0.07	0.01	-	0.01	0.01
K	0.02	-	-	-	0.02
Na	0.02	-	-	-	-
F	0.27	0.06	0.05	0.43	0.48

* except analyses from samples 23-2 and 199195

Numbers in parentheses are 1σ

** n.a. = not analysed

Table 9. Correlation matrix for REE in monazite

	Y	La	Ce	Pr	Nd	Sm	Gd
Y	1.00						
La	–0.02	1.00					
Ce	–0.18	–0.71	1.00				
Pr	–0.01	–0.82	0.57	1.00			
Nd	0.10	–0.89	0.50	0.82	1.00		
Sm	0.23	–0.60	0.23	0.44	0.69	1.00	
Gd	0.02	–0.29	–0.03	0.25	0.37	0.38	1.00

Monazite in sample 104361 from the marginal pegmatite was described in Karup-Møller *et al.* (2010), appearing as a patchy aggregate of crystals isolated in silicate minerals. Analyses of the lightest and darkest areas (Table 8 nos 2 and 3) of this aggregate gave the compositions (a): $(Ce_{0.46}La_{0.22}Pr_{0.04}Nd_{0.18}Sm_{0.03}Cd_{0.01})_{\sum 0.93}(P_{0.98}Si_{0.02})_{\sum 1.00}F_{0.01}O_{3.88}$ and (b): $(Ce_{0.47}La_{0.44}Pr_{0.02}Nd_{0.04}Sm_{0.01})_{\sum 0.98}P_{1.00}F_{0.01}O_{3.97}$ respectively. In Fig. 22, these compositions lie at the ends of the elongated monazite compositional range.

Monazite in sample 23-2 (circular pegmatite) and 199195 (marginal pegmatite) (Table 8 nos 4 and 5) have higher contents of La and correspondingly lower contents of Ce (Fig. 22). Monazite in sample 199195 represents the La-richest mineral recorded by us. It has the composition $(Ce_{0.26}La_{0.68}Pr_{0.01}Nd_{0.01})_{\sum 0.96}(P_{0.98}Si_{0.02})_{\sum 1.00}F_{0.05}O_{3.90}$.

Mineral A3 and associated minerals Uk2 and Uk3

Decomposition of the marginal area of a relatively large eudialyte crystal in sample 151428 has resulted in the formation of catapleiite as host for monazite and two previously undescribed minerals, A3 and Uk3. Two aggregates of A3 are present; one of these is shown in Fig. 23. The average chemical composition of 13 microprobe analyses of both aggregates is listed in Table 10 no. 1. A3 also occurs intergrown with Uk3 forming the aggregate shown in Fig. 24. The compositions of the two phases in this aggregate are listed in Table 10 nos 2 and 4.

In the analyses in Table 10 nos 1 and 2 the molar proportions for A3 are based on Si (+Ti) = 6.00. The average Si:REE is 6:2.78, i.e. close to 2:1, and quite different from that of A1 (1:1) and A2 (3:2). The oxide total is close to 80 wt%. A3 (like A2) is thus an OH/H_2O mineral with only small contents of F (A2 has no F). The following simplified formula for A3 is suggested: $Na_{0.2}Ca_{0.6}Mn_{0.5}Fe_{0.2}Al_{0.5}REE_{2.8}Si_{6.0}F_{0.5}O_{18-y}(OH)_{2y} \cdot nH_2O$.

The simplified formula for Uk3 is $CaCe_2(La,Pr,Nd,Sm,Gd)_2F_{0.2}O_{7-y}(OH)_{2y} \cdot nH_2O$. A phase with a similar composition has been identified in sample Gr2. Close to the decomposed eudialyte material in sample 151428, mineral Uk2 occurs as fracture fillings in fresh eudialyte (Fig. 25, Table 10 no. 3). It has a chemical composition $REE_{2.00}F_{1.50}O_{2.25-y}(OH)_{2y} \cdot nH_2O$, with Ce:(La+Pr+Nd+Sm+Gd)=1:1. It is almost identical with mineral Uk2 described by Karup-Møller *et al.* (2010). A phase with a similar composition has also

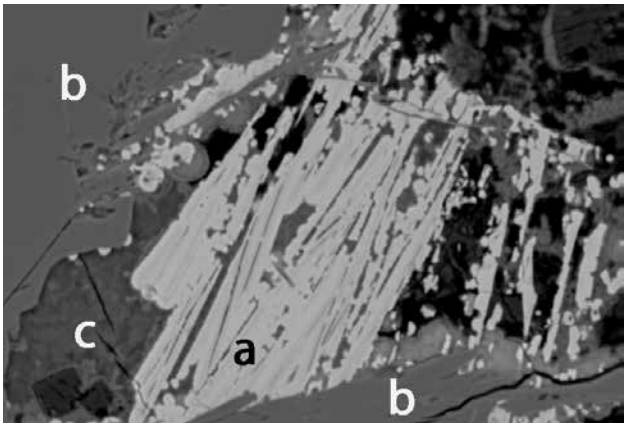

Fig. 23. Slightly radiating aggregate of mineral A3 crystals (a) in a matrix presumably of analcime (c) enclosed in catapleiite (b). Note the colloform texture of both analcime and A3 at upper left in the image. Sample 151428, circular pegmatite. Width of image 0.12 mm.

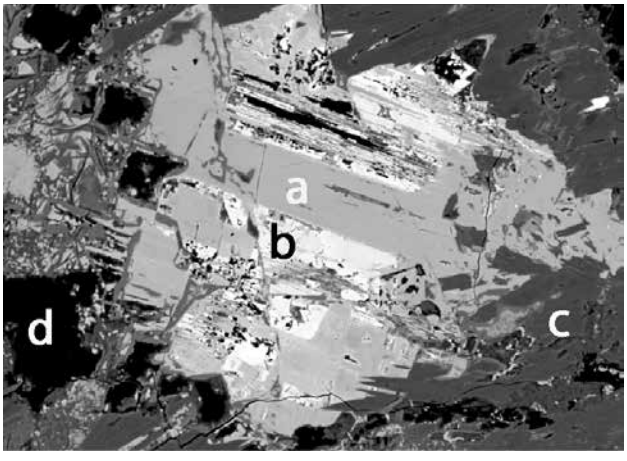

Fig. 24. Aggregate of mineral A3 (a) intergrown with mineral Uk3 (b) enclosed in catapleiite (c). Epoxy filled cavity at d. Sample 151428, circular pegmatite. Width of image 0.24 mm.

Table 10. Microprobe analyses of unidentified phases in sample 151428 (circular pegmatite)

	1	2	3	4
Mineral	A3	A3	Uk2	Uk3
No. of analyses	13	5	6	7
SiO_2	30.85 (1.43)	30.00 (.61)	-	0.20 (.06)
TiO_2	0.10 (.07)	0.11 (.03)	-	-
ZrO_2	- *	-	-	-
ThO_2	-	-	-	-
UO_2	-	-	-	-
P_2O_5	0.02 (.01)	0.02 (.01)	0.04 (.02)	0.03 (.03)
Al_2O_3	2.04 (.27)	2.14 (.14)	-	0.12 (.09)
Nb_2O_3	1.60 (.56)	1.62 (.09)	-	-
Y_2O_3	0.24 (.14)	0.42 (.20)	0.13 (.05)	0.06 (.05)
La_2O_3	10.08 (.70)	10.52 (.43)	21.57 (3.23)	17.78 (1.09)
Ce_2O_3	19.91 (.86)	17.93 (.38)	35.24 (1.13)	34.14 (1.35)
Pr_2O_3	1.90 (.22)	1.49 (.12)	2.94 (.26)	3.18 (.20)
Nd_2O_3	7.56 (.73)	5.90 (.40)	12.89 (1.83)	13.71 (.89)
Sm_2O_3	0.57 (.13)	0.51 (.09)	0.98 (.15)	1.32 (.24)
Gd_2O_3	0.12 (.14)	0.05 (.08)	0.40 (.20)	0.38 (.18)
Dy_2O_3	0.03 (.04)	0.12 (.14)	-	0.04 (.04)
Er_2O_3	-	-	0.10 (.10)	-
Yb_2O_3	0.04 (.06)	0.07 (.08)	0.14 (.15)	0.05 (.05)
FeO	1.17 (.26)	0.74 (.05)	-	-
MnO	2.61 (.65)	3.18 (.50)	-	-
CaO	3.00 (.26)	2.78 (.32)	0.45 (.08)	5.86 (.038)
K_2O	0.02 (.02)	0.02 (.01)	-	-
Na_2O	0.49 (.15)	0.49 (.02)	-	-
F	0.61 (.14)	0.79 (.06)	6.66 (.39)	0.45 (.14)
F–O corr.	–0.26	–0.33	–2.80	–0.19
Total	82.70	78.57	78.71	77.13
Atoms to	Si+Ti = 6.00	Si+Ti = 6.00	∑REE = 2.00	∑REE = 4.00
Si	5.98	5.98		0.04
Ti	0.02	0.02		
Al	0.47	0.51		0.02
Nb	0.14	0.15		
Y	0.02	0.05	0.01	0.01
La	0.73	0.77	0.59	1.02
Ce	1.42	1.31	0.95	1.94
Pr	0.13	0.11	0.08	0.18
Nd	0.52	0.42	0.34	0.76
Sm	0.04	0.04	0.02	0.07
Gd	0.01		0.01	0.02
∑REE	2.87	2.70	2.00	4.00
Fe	0.19	0.12		
Mn	0.43	0.53		
Ca	0.62	0.59	0.04	0.98
K				
Na	0.18	0.19		
F	0.38	0.50	1.54	0.22

* - = below detection limit Numbers in parentheses are 1σ

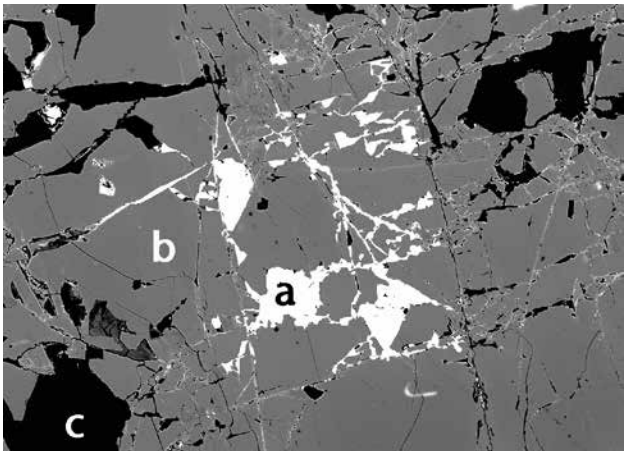

Fig. 25. Fractures in fresh eudialyte (b) filled with mineral Uk2 (a). Black areas (c) are either a silicate mineral (K-feldspar or analcime) or epoxy-filled cavities. Sample 151428, circular pegmatite. Width of image 0.61 mm.

been identified in samples from kakortokite layer –11 (Table 11 no. 5), 109304 and 230790.

Kainosite-(Y) and unknown Y-rich mineral Y1

In decomposed eudialyte in sample 151564 and kakortokite layer –11 we have identified two Y-rich minerals. One of these is assumed to be kainosite-(Y), while the other is assumed to be a new mineral species which has been termed Y1.

In Fig. 26 kainosite-(Y) is intergrown with catapleiite, and both minerals enclose Ca-poor A1 crystals. In addition aegirine and patches of K-feldspar are present. In other aggregates kainosite-(Y) (Table 11 no. 1) occurs intergrown with A1 and an unidentified Nb mineral (Karup-Møller & Rose-Hansen, unpublished data). The element oxide total recorded for kainosite-(Y) is close to 90 wt%. Assuming that the mineral is kainosite-(Y), i.e. a carbonate, then on the basis of the analysis in Table 11 no. 1 the following formula has been calculated: $(Ca,Fe,Na)_{1.99}(Y_{1.45}REE_{0.53})(SiO_3)_4CO_3{\cdot}H_2O$, or simplified $Ca_2Y_{1.5}REE_{0.5}(SiO_3)_4CO_3{\cdot}H_2O$.

Ca-poor A1 (Table 11 no. 2) often encrusts a phase which appears dark grey to nearly black in the microprobe images (Figs 27, 28). Microprobe analysis of this phase (Table 11 no. 3) yielded compositions close to that of the A1 host. The textural relations suggest that, as A1 crystallized, it enclosed material which subsequently crystallized as a distinct phase with a composition close to the host but enriched in Nb and Th. This phase presumably also contains OH/H_2O because the wt% oxide sum is slightly lower than that of the host.

Mineral Y1 was found in decomposed eudialyte in the sample from kakortokite layer –11. It forms a small aggregate enclosed in catapleiite. In the same catapleiite matrix we also found an aggregate of monazite (Fig. 29). The microprobe analysis of Y1 in this aggregate (Table 11 no. 4) is reported in wt% element values because it is not an oxide phase. Assuming that the missing anions are OH^- groups, then, on the basis of the analysis in Table 11 no. 4, the following simplified formula for Y1 is proposed: $Na_2Ca_4Y_{2.7}REE_{1.3}F_{18}(OH)_4$.

Discussion

Ca-rich and Ca-poor mineral A1

The two mineral A1-varieties have compositions resembling those of britholite: $(REE,Ca)_{10}(SiO_4,PO_4)_6(OH,F)_2$, britholite-(Ce): $Ca_4Ce_6(SiO_4)_6(OH)_2$ (Oberti *et al*. 2001) and lessingite-(Ce): $Ca_4REE_6(SiO_4)_6(OH,F)_2$. An unnamed mineral with the composition $NaCa_{1.5}REE_7(Si,P)_6O_{24}OH \cdot nH_2O$ described by Kalsbeek *et al*. (1990) is also regarded as a P_2O_5-poor member of the britholite group of minerals by these authors.

Britholite was originally found in South Greenland (Winther 1899). Since then, britholite has been found in several alkaline intrusions throughout the world. The mineral generally forms as a result of hydrothermal alteration (Arden & Halden 1999), although at the type locality it occurs as primary crystals in a nepheline syenite pegmatite at Naujakasik (Bøggild 1933). Britholite-(Ce) forms a solid solution series with apatite by the substitution of REE and Si for P and Ca (Khudolozhkin *et al*. 1973). Fully substituted britholite should then have the ideal composition $Ca_4REE_6(SiO_4)_6(F,OH)_2$, which actually is the composition of the now discarded lessingite-(Ce) (Burke 2006). Lessingite-(Ce) from the type locality at Kyshtym in Russia was described by Zilbermintz (1929) and restudied by Kalsbeek *et al*. (1990) who concluded that britholite-(Ce), lessingite-(Ce) and their unnamed mineral have the same crystal structure.

Britholite and related minerals belong to the apatite group with the general formula $M_{10}(ZO_4)_6X_2$ (M = Ca, Zr, Pb, Na…., Z = P, As, Si, V, REE…, and X = F, OH, Cl…). These minerals are tolerant to structural distortion and chemical substitution and are therefore extremely diverse in composition (e.g. Kreidler & Hummel 1970; McConnell 1973; Roy *et al*.1978; Elliott 1994). An extensive list of apatite group minerals and synthetic compounds with apatite structure is given by Pan & Fleet (2002). The X anions in the c-axis channels of natural apatites are dominated by F^-, OH^- and Cl^-. Additional substitutions in the c-axis anion channels include other monovalent anions (e.g. Br^-, I^-, O_2^-, O_3^-, BO_2^-, NCO^-, NO_3^- and NO_2^-) and divalent anions

Table 11. Microprobe analyses of kainosite and associated minerals

	1	2	3	4	5
Sample	151564	151564	151564	Layer–11	Layer–11
Mineral	Kainosite-(Y)	A1 (Ca-poor)	Phase enclosed in A1	Y1***	Uk2
No. of analyses	6	2	2	5	5
SiO_2	35.49 (.56)	23.97 (.13)	22.44 (.61)	-	0.03 (.02)
TiO_2	-*	0.17 (.03)	0.22 (.05)	-	-
ZrO_2	-	-	0.34 (.01)	-	-
ThO_2	0.14 (.09)	0.12 (.05)	2.66 (.01)	-	-
UO_2	0.05 (.03)	-	n.a.	-	0.03 (.02)
P_2O_5	-	0.14 (.06)	0.38 (.09)	-	0.02 (.02)
Al_2O3	-	0.58 (.15)	1.44 (.07)	-	-
Nb_2O_3	0.06 (.04)	0.07 (.03)	2.43 (.12)	0.04	-
Y_2O_3	24.22 (.81)	2.65 (.29)	3.09 (.01)	24.53	0.07 (.04)
La_2O_3	0.04 (.04)	17.97 (.05)	9.07 (.34)	0.50	17.69 (.38)
Ce_2O_3	0.15 (.14)	29.06 (.27)	24.10 (.32)	1.95	35.26 (.17)
Pr_2O_3	0.04 (.04)	2.30 (.15)	2.60 (.06)	0.63	3.15 (.21)
Nd_2O_3	0.34 (.19)	8.62 (.11)	12.06 (.05)	4.60	12.71 (.17)
Sm_2O_3	0.18 (.12)	2.12 (.02)	4.03 (.13)	1.80	1.62 (.28)
Gd_2O_3	2.18 (.23)	2.01 (.21)	3.13 (.39)	4.82	0.20 (.06)
Dy_2O_3	4.23 (.52)	n.a.**	n.a.	3.26	n.a.
Er_2O_3	4.35 (.28)	n.a.	n.a.	1.29	n.a.
Yb_2O_3	3.02 (.44)	n.a.	n.a.	0.32	n.a.
FeO	0.02 (.02)	1.22 (.04)	1.00 (.06)	-	-
MnO	-	0.23 (.06)	0.52 (.24)	-	-
CaO	14.84 (.28)	3.92 (.10)	3.29 (.13)	16.25	-
K_2O	-	-	-	-	-
Na_2O	0.40 (.14)	-	-	4.55	-
F	-	1.20 (.16)	1.20 (.16)	33.84	6.82 (.37)
F–O corr.	-	–0.51	–0.51	-	–2.87
Total	89.75	95.84	93.49	98.38	74.73
Atoms to	Si = 4.00	Si+Ti = 6.0	Si+Ti+Zr = 6.0	Ca = 4.00	∑REE =2.00
Si	4.00	5.97	5.91		
Ti		0.03	0.04		
Zr			0.04		
Th			0.16		
U					
P		0.03	0.09		
Al		0.17	0.45		
Nb		0.01	0.29		
Y	1.45	0.35	0.43	2.72	
La		1.68	0.88	0.04	0.51
Ce	0.01	2.65	2.33	0.14	1.00
Pr		0.21	0.25	0.04	0.09
Nd	0.02	0.77	1.14	0.31	0.35
Sm	0.01	0.18	0.37	0.12	0.04
Gd	0.08	0.17	0.27	0.30	0.01
Dy	0.15			0.20	
Er	0.15			0.08	
Yb	0.11			0.02	
∑REE	1.98	6.01	5.67	3.97	2.00
Fe		0.25	0.22		
Mn		0.05	0.10		
Ca	1.79	1.05	0.93	4.00	
K					
Na	0.09			1.95	
F	-	0.78	1.01	17.56	1.67

* - = below detection limit ** n.a. = not analysed ***element values, not oxides

Numbers in parentheses are 1σ

(O^{2-}, CO_3^{2-}, O_2^{2-}, S^{2-}, HCN^{2-} and NO_2^{2-}), vacancy (□), and neutral and organic molecules (McConnel 1973; Trompe & Montel 1978; Elliott 1994). A large number of divalent, trivalent, tetravalent and hexavalent cations may substitute for Ca^{2+}. Ca-deficiency has been reported to occur in both natural and synthetic apatites. Assuming that Ca-rich A1 with 25 mol % Ca less than in ideal britholite has the apatite structure, the following substitution may have taken place: $Ca^{2+}+F^{-} = H^{+}+$ □ and the formula would then be: $HCa_3REE_6(SiO_4)_6(F□)$, with Si:REE = 1:1.

The Ca-poor A1 has a significantly lower Si:REE ratio than Ca-rich A1. It is not possible to demonstrate substitutional relationships involving anion vacancies and still maintain the apatite structural scheme for this mineral. We therefore conclude that Ca-poor A1 does not have the apatite structure. At present the following simplified empirical formula for the mineral is proposed: $(Fe,Mn,Ca)_{1.5}REE_6Si_6FO_{22}$ until the mineral is found with a sufficiently large crystal size to allow its structure to be determined.

It is evident from Fig. 11 that Ce remains almost independent of the substitutional relationships between the other REE, in particular La and Nd, in the crystal structure of both A1 varieties and to some extent also in monazite (Fig. 22). Furthermore Ce, in contrast to the other REE, may occur with both valences +3 and +4. Alteration of eudialyte may have taken place under

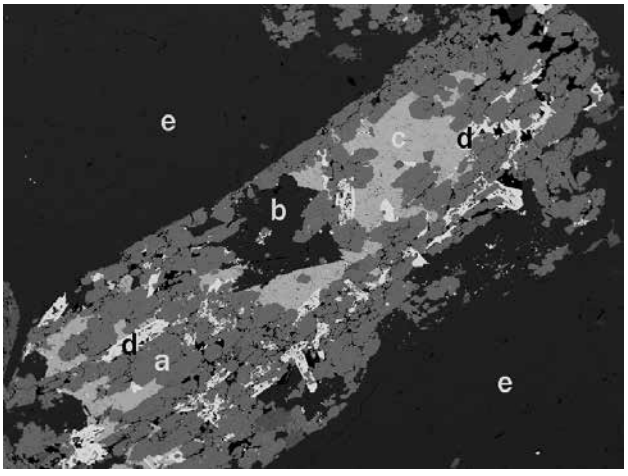

Fig. 26. Eudialyte decomposition aggregate composed of catapleiite (a), kainosite-(Y) (c), Ca-poor A1 (d) and K-feldspar and analcime (b) isolated in a fine-grained albite matrix (e). Note that aegirine is absent from the decomposition aggregate. Sample 151564, aegirine pegmatite sill. Width of image 1.47 mm.

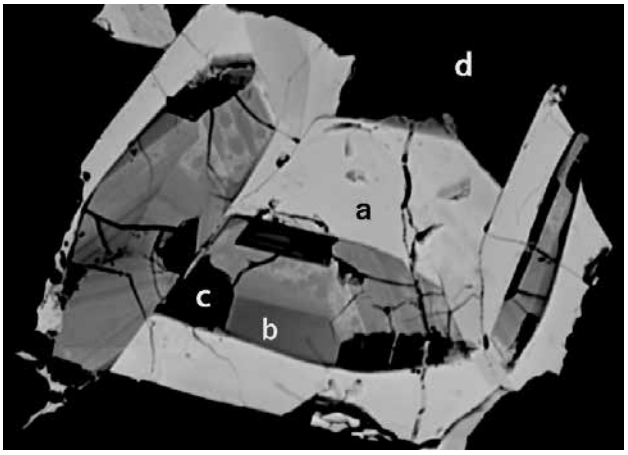

Fig. 27. Aggregate of Ca-poor A1 crystals (a) enclosing a phase with composition near A1 (b). The black areas (c) are either a silicate mineral (analcime or K-feldspar) or epoxy-filled cavities. The host (d) is catapleiite. Sample 151564, aegirine pegmatite sill. Width of image 0.13 mm.

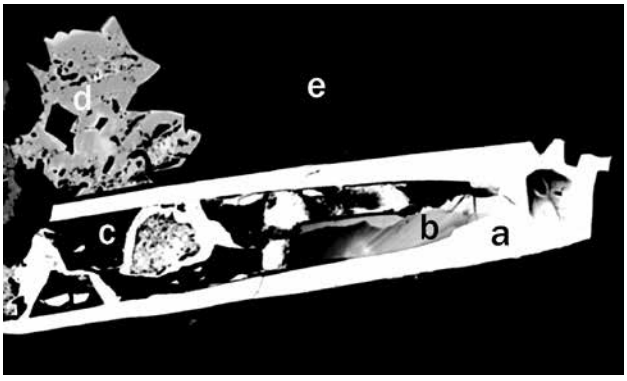

Fig. 28. Ca-poor A1 crystal (a) enclosing an A1-like phase (b) and epoxy-filled cavities or an unidentified silicate mineral (c) in contact with an unidentified REE-mineral (d), all enclosed in catapleiite (e). Similar A1 crystals are enclosed in the eudialyte decomposition aggregate shown in Fig. 26. Sample 151564, aegirine pegmatite sill. Width of image 0.25 mm.

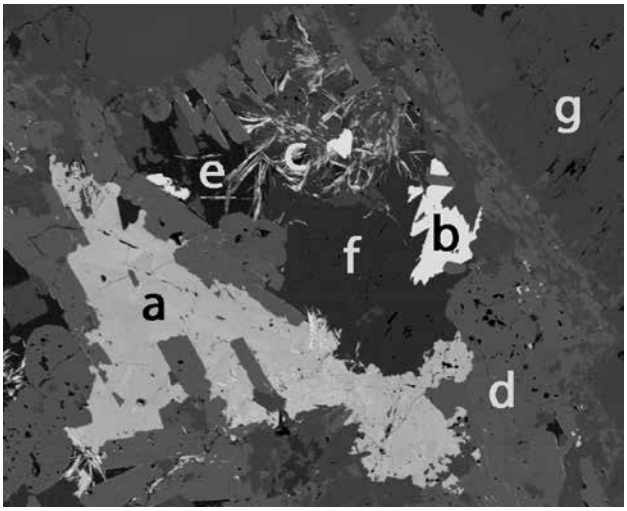

Fig. 29. Eudialyte decomposition aggregate composed of an aggregate of mineral Y1 crystals (a), an aggregate of monazite crystals (b), thin A1-crystals (c), catapleiite (d), K-feldspar (f) and analcime (e), enclosed in aegirine (g). Kakortokite layer –11. Width of image 0.90 mm.

oxygen fugacities sufficiently high to allow for the formation of Ce^{4+}. However it is not very likely that the Ce^{4+} ion, because of its small ionic radius (0.97 Å for Ce^{4+} versus 1.14 for Ce^{3+}, Shannon 1976), may exist in the apatite structure type although it is common in zircon (Thomas *et al*. 2003). The ionic radius of Zr^{4+} is 0.87 Å. However, assuming that one Ce atom per formula unit of Ca-rich A1 has a valence of +4, then this would require one empty cation position and one empty anion position per formula unit. With two Ce^{4+} cations per formula unit, one empty cation position is still required but no empty anion positions.

Assuming that Ca-poor A1 also has apatite structure, then 2.5 Me^{2+} per formula unit are 'missing'. However, there are only about 3 Ce atoms per formula unit. Assuming that all three Ce atoms have a valence of +4, then one Me^{2+} would still be missing. This could be resolved by having one half empty position plus two 'empty' Me^{2+} occupied by H^+, and fully occupied anion positions per formula unit. Under these assumptions the following two formulae for Ca-rich A1 and one for Ca-poor A1 can be proposed:

Ca-rich A1: $\square Ca_3Ce^{4+}REE_5(SiO_4)_6(F\square)$

Ca-rich A1: $\square Ca_3Ce_2^{4+}REE_4(SiO_4)_6(F,OH)_2$

Ca-poor A1: $\square_{0.5}H_2(Fe,Mn,Ca)_{1.5}Ce_3^{4+}REE_3(SiO_4)_6(F,OH)_2$

Ca-poor A1 enriched in Nb, Th, Ti and Al

All mineral A1 studied, except for in sample 23-2, are formed from the decomposition of eudialyte. Eudialyte has no detectable amounts of P, and this may explain why mineral A1 contains very little of this element, although monazite is an accessory mineral in some aggregates. However, in sample 23-2 Ca-poor A1 in association with catapleiite and an unidentified Nb-mineral was precipitated in cavities after an unknown mineral, presumably the water-soluble mineral villiaumite (NaF). Early precipitated mineral A1 contains considerable amounts of P and Na but only small amounts of Ca, Nb and Th and almost no aluminium. As the precipitation of minerals continued, late solutions may have reacted with early precipitated mineral A1 in these cavities resulting in the formation of hydrated mineral A1 varieties with up to 8.23 wt% ThO_2, 6.61 wt% Nb_2O_5, 1.77 w.% Al_2O_3, 1.61 wt% CaO and 0.98 wt% TiO_2. At the same time the contents of P and Na were strongly reduced. However, in all phases the Si+P to REE molar ratio remained virtually unchanged, close to 1:1. This suggests that the Ca-poor A1 structure type allows substantial substitutions as is the case for the apatite structure type.

Distribution of REE

During decomposition the majority of REE in the original eudialyte were concentrated mainly in mineral A1 and to some extent also in mineral A2. The other unidentified REE minerals play a subordinate role in this respect as they are present in insignificant amounts. Yttrium, however, plays a major role in the formation of the secondary minerals where Y is mainly concentrated in fergusonite-(Y), mineral A2, kainosite-(Y) and mineral Y1. Relatively little Y is present in mineral A1 compared to the amount contained in the original eudialyte (Fig. 11b, d).

Eudialyte contains practically no P; nevertheless in some decomposition aggregates both monazite and apatite have been identified. P must therefore have been introduced during the decomposition process from an external source.

A characteristic feature of nearly all the secondary minerals (except for kainosite-(Y) and mineral Y1) is that Ce constitutes nearly half the amount of REE present. This is also valid for the original eudialyte. For mineral A1, most of the analyzed monazite grains, and to some extent mineral A2, extensive exchange can take place between La on one hand and Pr, Nd, Sm and Gd on the other (Figs 11, 21, 22). In mineral A1 and some monazite grains, increasing content of La is accompanied by a slight increase in the content of Ce. In mineral A2 there is a more pronounced increase in the content of Ce with increasing content of La and decreasing contents of the other REE. A similar element relationship is only vaguely seen in the original eudialyte. Here increasing content of La is accompanied by increasing content of Nd and decreasing amounts of Pr, Sm and Gd. At the same time increasing contents of La and Nd are accompanied by a significantly stronger increase in the content of Ce compared to mineral A1. This is also indicated by the shape of the eudialyte compositional field in Fig. 11a.

Conclusions

The major alteration mineral of eudialyte from the kakortokite part of the Ilímaussaq complex is catapleiite. Generally the shapes of the original eudialyte crystals are perfectly preserved (e.g. the eudialyte pseudomorph in Fig. 26). It appears that the original element content in the eudialyte is preserved within the eudialyte pseudomorphs. Zirconium is contained in catapleiite. The major part of the REE are concentrated in mineral A1, locally also in fergusonite-(Ce), fergusonite-(Y), monazite, and minerals A2, A3, Uk2 and Uk3. Detailed analyses of mineral A1, originally described by Karup-Møller *et al*. (2010), have proved

the existence of two varieties: Ca-rich and Ca-poor A1. The Ca-rich variety, close in composition to 'lessingite' but with pronounced cation deficiency, has the ideal formula $HCa_3REE_6(SiO_4)_6(F\square)$ and may possess apatite structure; hence it may be a member of the britholite group. The chemically related Ca-poor A1 variety appears not to be a member of the same group. Mineral Uk2, originally described by Karup-Møller *et al*. (2010) and found only in one sample (locality C, Fig. 1) has been found during the present investigation at three additional localities.

The proportion between Ce and the other REE is close to 1:1 both in the original eudialyte and in the secondary minerals. Characteristic for all secondary minerals is a significant substitutional relationship between La on one hand and Nd, Pr, Sm, Gd (and presumably also the minor amounts of HREE) on the other. For mineral A1 (both varieties, but in particular for Ca-rich A1), there is a slight increase in the content of Ce with increasing content of La and decreasing content of Nd, Pr, Sm and Gd. This is substantial for mineral A2. For monazite the Ce content remains constant. A similar well-defined relationship for the REE in eudialyte cannot be recognized. Here the substitutional relationships between these elements are much less pronounced and they also show different trends (Fig. 11a).

Chlorine in the secondary minerals is below the detection limit, and this element must have been removed during the decomposition of eudialyte. In contrast, P which is absent in eudialyte must have been added to those decomposition aggregates which contain monazite and apatite.

The proportion between Y and the other REE is significantly higher in eudialyte than in mineral A1 (Fig.11b). This may explain the formation of fergusonite-(Y), mineral A2 and locally the two Y minerals kainosite-(Y) and Y1. Kainosite constitutes a significant proportion of the decomposition aggregate shown in Fig. 26. The original eudialyte in this sample may therefore have had an Y content above the average for this mineral.

Acknowledgements

We are grateful for the technical assistance of A. Berger, M.K. Sørensen and H. Diaz. E. Makovicky, J.C. Bailey, T. Balic-Zunic and H. Friis read the manuscript and made valuable comments on its contents. The English was checked by J.C. Bailey. Collaboration with H. Bohse in the field is greatly appreciated. The Danish Natural Science Research Council provided the microprobe facilities.

References

Andersen, S., Bailey, J.C. & Bohse, H. 1981: Zr-Y-U stratigraphy of the kakortokite-lujavrite-sequence, southern Ilímaussaq intrusion. Rapport Grønlands Geologiske Undersøgelse 103, 69–76.

Andersen, S., Bohse, H. & Steenfelt, A. 1988: The southern part of the Ilímaussaq complex, South Greenland, 1:20.000 geological map. Copenhagen: Geological Survey of Greenland.

Arden, K.M. & Halden, N.M. 1999: Crystallization and alteration history of britholite in rare-earth-element-enriched pegmatitic segregations associated with the Eden Lake Complex, Manitoba, Canada. Canadian Mineralogist 37, 1239–1253.

Bailey, J.C. 1995: Cryptorhytmic and macrorhytmic layering in aegirine lujavrite, Ilímaussaq alkaline intrusion, South Greenland. Bulletin of the Geological Society of Denmark 42, 1–16.

Bøggild, O.B. 1933: Igalikite and naujakasite, two new minerals from South Greenland. Meddelelser om Grønland 92(9), 12 pp.

Bohse, H. & Andersen, S. 1981: Review of the stratigraphic divisions of the kakortokite and lujavrite in southern Ilímaussaq. Rapport Grønlands Geologiske Undersøgelse 103, 53–61.

Bohse, H., Brooks, C.K. & Kunzendorf, H. 1971: Field observations on the kakortokites of the Ilímaussaq intrusion, South Greenland, including mapping and analyses by portable X-ray fluorescence equipment for zirconium and niobium. Rapport Grønlands Geologiske Undersøgelse 38, 43 pp.

Bohse, H., Rose-Hansen J., Sørensen, H., Steenfelt, A., Løvborg, L. & Kunzendorf, H. 1974: On the behavior of uranium during crystallization of magma – with special emphasis on alkaline magmas. In: Formation of Uranium Ore Deposits, 49–60.Vienna: International Atomic Energy Agency.

Burke, E.A.J. 2006: A mass discreditation of GQN minerals. Canadian Mineralogist 44, 1557–1560.

Elliott, J.C. 1994: Structure and chemistry of the apatites and other calcium orthophosphates, 387 pp. Amsterdam: Elsevier.

Ferguson, J. 1964: Geology of the Ilímaussaq alkaline intrusion, South Greenland. Description of map and structure. Bulletin Grønlands Geologiske Undersøgelse 39, 82 pp.

Gerasimovsky, V.I. 1969: Geochemistry of the Ilímaussaq alkaline massif (South-west Greenland). (Geochimija Ilimmassakskogo stselotsnogo massiva (Jugo-sapadnaja-Greenlandija), 174 pp. Moscow: Nauka. (in Russian).

Graser, G. & Markl, G. 2008: Ca-rich ilvaite-epidote-hydrogarnet endoskarns: a record of late-magmatic fluid influx in the persodic Ilímaussaq complex, South Greenland. Journal of Petrology 49, 239–265.

Henriksen, J.H.H. 1993: Geochemical trends through part of the upper transitional kakortokites and aegirine lujavrite I, Ilímaussaq intrusion, South Greenland. Unpublished M.Sc. thesis, University of Copenhagen, 185 pp.

Johnsen, O. & Bohse, H. 1981: Helvine from the Ilímaussaq intrusion. In: Bailey, J.C., Larsen, L.M. & Sørensen, H. (eds): The

Ilímaussaq intrusion, South Greenland. A progress report on geology, mineralogy, geochemistry and economic geology. Rapport Grønlands Geologiske Undersøgelse 103, 25–29.

Johnsen, O. & Grice, J.D. 1999: The crystal chemistry of the eudialyte group. Canadian Mineralogist 37, 865–891.

Kalsbeek, N., Larsen, S. & Rønsbo, J.G. 1990: Crystal structures of rare earth elements rich apatite analogues. Zeitschrift für Kristallographie 191, 249–263.

Karup-Møller, S. 1975: On the occurrence of the native lead, litharge, hydrocerussite and plattnerite from the Ilímaussaq alkaline intrusion in South Greenland. Neues Jahrbuch für Mineralogie, Monatshefte 5, 229–241.

Karup-Møller, S. 1982: Tundrite from the Ilímaussaq alkaline intrusion, South Greenland. Neues Jahrbuch für Mineralogie, Monatshefte 481–494.

Karup-Møller, S., Rose-Hansen, J. & Sørensen, H. 2010: Eudialyte decomposition minerals with hitherto undescribed phases from the Ilímaussaq complex, South Greenland. Bulletin of the Geological Society of Denmark 58, 75–88.

Khudolozhkin, O., Urusov, V.S. & Tobelko, K.I. 1973: Dependence of structural ordering of rare earth atoms in the isomorphous series apatite-britholite (abukumalite) on composition and temperature. Geochemistry International 10, 1171–1177.

Kreidler, E.R. & Hummel, F.A. 1970: The crystal chemistry of apatite: structure fields of fluor- and chlorapatite. American Mineralogist 55, 170–184.

Macdonald, R., Karup-Møller, S. & Rose-Hansen, J. 2007: Astrophyllite-group minerals from the Ilímaussaq complex, South Greenland. Mineralogical Magazine 71, 1–16.

McConnel, D. 1973: Apatite, its crystal chemistry, mineralogy, utilization, and geologic and biologic occurrences, 111pp. New York: Springer.

Oberti, R., Ottolini, L., Della Ventura, G. & Pardon, G.C. 2001: On the symmetry and crystal chemistry of britholite. New structural and microanalytical data. American Mineralogist 86, 1066–1075.

Pan, Y. & Fleet, M.E. 2002: Compositions of the apatite-group minerals: substitution mechanisms and controlling factors. Reviews in Mineralogy and Geochemistry 48, 13–49.

Pfaff, K., Krumrei, T.H. Marks, M., Wenzel, T.R. & Markl, G. 2008: Chemical and physical evolution of the "lower layered sequence" from the nepheline syenitic Ilímaussaq intrusion, South Greenland: Implications for the origin of magmatic layering in peralkaline felsic liquids. Lithos 106, 280–296.

Rose-Hansen, J. & Sørensen, H. 2002: Geology of the lujavrites from the Ilímaussaq alkaline complex, South Greenland, with information from seven bore holes. Meddelelser om Grønland, Geoscience 40, 58 pp.

Roy, D.M., Drafall, L.E. & Roy, R. 1978: Crystal chemistry, crystal growth, and phase equilibria of apatites. In: Alper, A.M. (ed.), Phase Diagrams, Material Sciences and Technology 6-V, 186–239. New York: Academic Press.

Shannon, R.D. 1976: Revised effective ionic radii and systematic studies of interatomic distances in halides and chalcogenides. Acta Crystallographica A 32, 751–767.

Sørensen, H. 1960: On the agpaitic rocks. Report 21st International Geological Congress Norden 1960 vol. 13, 319–327.

Sørensen, H. 1962: On the occurrence of steenstrupine in the Ilímaussaq massif, Southwest Greenland. Meddelelser om Grønland 167(1), 251 pp.

Sørensen, H. 1992: Agpaitic nepheline syenites: a potential source of rare elements. Applied Geochemistry 7, 417–427.

Sørensen, H. 2006: The Ilímaussaq alkaline complex, South Greenland. An overview of 200 years of research and an outlook. Meddelelser om Grønland, Geoscience 45, 1–70.

Sørensen, H., Rose-Hansen, J., Nielsen, B.L., Løvborg, L., Sørensen, E. & Lundgaard, T. 1974: The uranium deposit at Kvanefjeld, the Ilímaussaq intrusion, South Greenland. Geology, reserves and beneficiation. Rapport Grønlands Geologiske Undersøgelse 60, 54 pp.

Sørensen, H., Bohse, H. & Bailey, J.C. 2006: The origin and mode of emplacement of lujavrites in the Ilímaussaq alkaline complex, South Greenland. Lithos 91, 286–300.

Thomas, J.B., Bodnar, R.J., Shimizu, N. & Chesner, C.A. 2003: Melt inclusions in zircon. Reviews in Mineralogy and Geochemistry 53, 63–87.

Trompe J.C. & Montel, G. 1978: Some features in the incorporation of oxygen in different oxidation stages in the apatite lattice–II. On the synthesis and properties of calcium and strontium peroxiapatites. Journal of Inorganic Nuclear Chemistry 40, 23–26.

Ussing, N.V. 1898: Mineralogisk-petrografiske undersøgelser af grønlandske Nefelinsyenitter og beslægtede Bjergarter. Meddelelser om Grønland 14, 1–220.

Ussing, N.V. 1912: Geology of the country around Julianehaab, Greenland. Meddelelser om Grønland 38, 376 pp.

Westergaard, A.S. 1969: The border pegmatites of the Ilímaussaq intrusion. Rapport Grønlands Geologiske Undersøgelse 19, 39–40.

Winther, C. 1899: In: Bøggild, O.B. & Winther, C.: On some minerals from the nephelite-syenite at Julianehaab, Greenland (epistolite, britholite, schizolite and steenstrupine), collected by G. Flink. Meddelelser om Grønland 24, 181–213.

Zilbermintz, V.A. 1929: Sur le gisement de cérite, de bastnesite et d'un minéral nouveau la lessingite, dans le district Minier, Kychtym (Ural). Doklady Akademii. Nauk SSSR A3, 55–60.